NAS1.60:1031

SEP 21 1977

NASA Technical Paper 1031

COMPLETED
ORIGINAL

Effects of Temperature Transients at Fan Inlet of a Turbofan Engine

Mahmood Abdelwahab

SEPTEMBER 1977

NASA

41

NASA Technical Paper 1031

Effects of Temperature Transients at Fan Inlet of a Turbofan Engine

Mahmood Abdelwahab

Lewis Research Center
Cleveland, Ohio

National Aeronautics
and Space Administration

**Scientific and Technical
Information Office**

1977

EFFECTS OF TEMPERATURE TRANSIENTS AT FAN INLET OF A TURBOFAN ENGINE

by Mahmood Abdelwahab

Lewis Research Center

SUMMARY

An experimental investigation was conducted to determine the effects of fan inlet, time-dependent, total temperature distortion on the performance and stability of a TF30-P-3 turbofan engine. Time-dependent distortions were produced by a gaseous-hydrogen-fueled burner system installed upstream of the fan inlet. Data were obtained at a fan inlet Reynolds number index of 0.50 and at 90 and 74 percent of low-pressure-rotor military speed (9525 rpm). At each engine condition, tests were conducted with 90°, 180°, 270°, and 360° of the fan inlet circumferential extent exposed to a range of magnitudes and rates of temperature rise.

The engine response to temperature transients was characterized by the reaction of the compressor system. The compressor response ranged from a momentary compressor pressure disturbance to low-pressure-compressor stall, depending on the severity of the distortion.

The compressor distortion limits, in terms of the magnitude and rate of fan inlet temperature change required to produce compressor stall, decreased with decreasing low-pressure-rotor speed and increased with increasing circumferential extent of distortion. For example, with 90° circumferential extent of distortion, the distortion limits decreased from a temperature rise rate of 2222 K per second and a peak temperature change of 70 K to 1834 K per second and 59 K as the low-pressure-rotor speed was reduced from 90 percent to 74 percent. At 90-percent low-pressure-rotor speed, the limits increased from 2222 K per second and 70 K to 3833 K per second and 117 K as the circumferential extent of distortion was increased from 90° to 360°. The magnitude and rate of fan inlet temperature change were directly related in this experiment as a result of the hydrogen burner design used. However, analysis of the data obtained with 180°-extent distortion at both low-pressure-rotor speeds suggests strongly that the distortion limits of the compressor are a function of a critical magnitude of fan inlet temperature rise and are independent of the temperature rise rate.

During transients at 90-percent low-pressure-rotor speed in which stall did not occur, it was observed that the hot gases at the fan inlet swirled circumferentially more than 120° in the direction of rotor rotation as they passed from the fan inlet to the high-pressure-compressor exit.

INTRODUCTION

An experimental investigation was conducted to determine the effects of fan inlet, time-dependent, total temperature distortion on the performance and stability of a production TF30-P-3 turbofan engine. Typically, time-dependent temperature distortion at the engine inlet can occur as a result of hot gas ingestion by the engine during, for example, armament firing, thrust reversal, and takeoff and landing by VTOL and STOL aircraft. Although the total problem of hot gas ingestion is very complex and involves many factors, rapid engine inlet temperature rises are probably the principal factor affecting the performance and stability limits of the engine. Therefore, an investigation of the effects that temperature transients have on engines will add to knowledge and understanding of the problem and could provide information leading to its alleviation and/or elimination.

Most earlier investigations of engine inlet temperature transients were conducted on turbojet engines (refs. 1 to 3). In reference 1, it was concluded that compressor stall occurred before the inlet temperature had risen 56 K (100° R), with a temperature rise rate of 3025 K per second (5000° R/sec) and a circumferential extent of distortion of 360°. Also, it was found that the engine could withstand larger inlet temperature rises (at the same rise rate) prior to stall if the distortion covered less than 360° of the inlet circumferential extent. Very little information was found in the literature concerning the effects of inlet temperature transients on turbofan engines. Rudey and Antl (ref. 4) reported the effects of time-dependent temperature distortion on an experimental two-spool turbofan engine and concluded that the rate of change in engine inlet temperature had a more pronounced effect than either the circumferential extent of distortion or the magnitude of temperature rise obtained during a transient. The investigation reported herein was conducted to extend our knowledge of the independent effects that the principal variables involved in inlet temperature transients have on the performance and stability of an engine. Some of these variables are the rate and magnitude of inlet temperature change, the circumferential extent of distortion, and low-pressure-rotor speed. Also, an attempt was made to identify the types of compressor responses obtained with increasingly higher temperature rises and to separate the effects of the magnitude and rate of the inlet temperature change on the compressor distortion limits.

The experiment was conducted in an altitude test facility on a twin-spool, low-bypass-ratio turbofan engine equipped with an afterburner. The temperature transients were generated by a gaseous-hydrogen-fueled burner installed upstream of the engine inlet. The transients were controlled by varying the flow rate of a fixed volume of hydrogen and thus the magnitude and rate of the inlet temperature change. Data were obtained at a fan inlet Reynolds number index RNI of 0.50 and at 90 and 74 percent of the low-pressure-rotor military speed. At each condition, tests were conducted with 90°, 180°, 270°, and 360° of the fan inlet circumferential extent exposed to a range of peak

temperature magnitudes and temperature rise rates.

APPARATUS

Engine

The engine used for this investigation was a production TF30-P-3 twin-spool turbofan engine equipped with an afterburner and 7th- and 12th-stage bleeds. The engine was installed in an altitude test chamber by a direct-connect type of installation (fig. 1).

Distortion Device

The gaseous-hydrogen-fueled burner device used to produce the time-dependent temperature distortion was installed upstream of the engine inlet bellmouth (figs. 2 and 3). The burner duct was divided into four quadrants. Air passing through the burner duct was heated in selected 90° sectors. Each 90° sector of the burner and associated hydrogen system consisted of five swirl-can pilot burners to provide the ignition source for the hydrogen; five annular gutters supported by one radial gutter; five circular tube-manifolds (one inside each annular gutter) with small holes for hydrogen injection; one hydrogen manifold located outside the burner duct and connected to the five circular tubes by tubing; and a high-response valve and a flow control valve, which were used to connect the hydrogen manifold to the hydrogen supply source. The control system for each quadrant could open the high-speed valve to start the flow of hydrogen, which had been trapped between the high-speed valve and the control valve prior to a transient, into the quadrant. The four sectors and their control systems were identical. The high-response valves could be energized in any desired combination at the same time.

Instrumentation

The engine was instrumented as shown in figure 1. Steady-state and dynamic total pressures, static pressures, and total temperatures were measured and recorded. Steady-state pressures between 0 and 24 N/cm^2 were recorded on a digital automatic multiple-pressure recorder. High-level pressures were measured by means of a Scanivalve system. Steady-state temperatures were measured by using Chromel-Alumel thermocouples. Both the high-level pressures and the steady-state temperatures were recorded on an automatic voltage digitizer.

Dynamic pressure measurements were made by using miniature strain-gage transducers capable of at least 300-hertz frequency response. A more complete discussion of this type of instrumentation is given in reference 5. Chromel-Alumel thermocouples made from 7.6-millimeter- (0.003-in.-) diameter wires were used to measure the transient total temperatures. These thermocouples were installed in the following locations (fig. 1):

Station	Angular location, deg
2a	18, 63, 108, 153, 198, 243, 288, 333
2.3	56
2.3f	56
3	60
4	120

All other thermocouples shown in figure 1 were steady state. The indicated temperatures from these thermocouples were corrected for ram recovery and time lag based on steady-state data recorded before each transient. The methods used for these corrections are given in appendix B. (Symbols are defined in appendix A.)

High-response pressure data were recorded on an analog data-recording system. These data were digitized at a rate of 1000 samples per second by using a 500-hertz low-pass filter. Dynamic total temperature data were recorded and digitized on a high-speed sequential digital system at a rate of 100 samples per second. One low-pressure-compressor exit dynamic total pressure ($P_{t,\,3\text{-}118^{\circ}\text{-}2}$) was recorded on both the analog and the high-speed digital systems. This pressure was used to correlate time between the two systems. (The notation $3\text{-}118^{\circ}\text{-}2$, for example, denotes the station (3), the circumferential position (118°), and the radial position of the probe (2). This notation is used throughout this report.)

PROCEDURE

For this investigation, the fan inlet pressure and temperature were set prior to each transient to maintain Reynolds number index at 0.50. The pretransient fan inlet temperature was at approximately 39 K. Tests were conducted at low-pressure-rotor speeds N_1 of 90 and 74 percent of the military value (9525 rpm). At each engine condition, data were obtained with 90°, 180°, 270°, and 360° circumferential extents of the fan inlet exposed to a range of peak temperature magnitudes and temperature rise rates.

A steady-state data point was recorded when the test conditions had been established and the data systems readied. A desired hydrogen pressure was established in the volume between the flow control valve and the high-speed valve for the specified quadrants. The swirl-can ignitors at those quadrants were then lit. The high-speed digital and the analog data systems were activated, and the high-speed valves in the selected quadrants were remotely opened electrically. Hydrogen was burned, giving a temperature rise rate in the specified fan inlet quadrants. The rate and magnitude were a function of the quantity of trapped hydrogen, which was indicated by the pressure. The pressure of the trapped hydrogen was increased and the process repeated until a compressor stall limit was reached. Because the hydrogen burner was a constant-volume system, the magnitude and rate of the fan inlet temperature change were directly related.

RESULTS AND DISCUSSION

The effects of fan inlet, time-dependent, total temperature distortion were investigated at a fan inlet Reynolds number index of 0.50 and at 90 and 74 percent of low-pressure-rotor military speed. Varying degrees of distortion severity were imposed at 90°, 180°, 270°, and 360° circumferential extents of the fan inlet at each engine condition. The results are presented and discussed under three categories: (1) fan inlet flow conditions during the transients and prior to compressor stall, (2) engine response, and (3) compressor distortion limits.

Fan Inlet Conditions

To better understand the effects of time-dependent temperature distortion produced by the hydrogen burner system on the performance and stability of the engine, the fan inlet flow conditions during the transients and prior to compressor stall should be defined. These conditions serve to identify the inlet variables affecting the engine response and its tolerance to distortion. For this purpose, data are presented for transients of 90°, 180°, 270°, and 360° circumferential extents Ψ at 90-percent N_1 in terms of time histories of circumferential and radial inlet temperatures, instantaneous contour maps of inlet temperature prior to stall, instantaneous circumferential inlet temperature patterns, inlet pressure, and a pressure distortion parameter. The inlet flow conditions presented are also typical of those obtained during transients at 74-percent N_1.

Time-history profiles of circumferential and radial fan inlet temperatures are presented in figure 4. The circumferential temperature profiles (fig. 4(a)) represent data obtained from the middle thermocouple probe (probe 3) of each fan inlet (station 2a) temperature rake. The radial temperature profiles (fig. 4(b)) represent data obtained from

the individual probes of the rakes at angular locations θ of 63°, 108°, 333°, and 243° for temperature distortions having circumferential extents of 90°, 180°, 270°, and 360°, respectively. It is apparent from these profiles that the time-dependent temperature distortions produced by the hydrogen burner system contained circumferential and radial variations in temperature rise rate, as well as instantaneous spatial (circumferential and radial) distortion, prior to compressor stall. For example, for the 360°-extent transient (fig. 4(a-4)), the temperature rise rate varied circumferentially from 5300 K per second at $\theta = 288^{\circ}$ to 3350 K per second at $\theta = 18^{\circ}$. Radially, it varied from 3400 K per second at an inlet passage height of 41.8 percent to 3050 K per second at 92.2 percent. The absolute value of instantaneous temperature at 50 milliseconds varied circumferentially from 442 K at $\theta = 153^{\circ}$ to 386 K at $\theta = 198^{\circ}$ and radially from 400 K at an inlet passage height of 78.4 percent to 378 K at 16.8 percent. These temperature rise rates represent the initial, nearly linear, maximum temperature rise rate (fig. 4(a-4)); the method used for calculating it is described in appendix C.

The combined characteristics of the circumferential and radial variations in fan inlet absolute temperature during 90°, 180°, 270°, and 360° circumferential-extent transients are shown in figure 5 as isotherms at the compressor face (station 2a) approximately 20 milliseconds before compressor stall. The maps were generated by the method of reference 6. The dashed circular lines shown on the maps represent the split between the fan and core flow areas projected from station 2.3. The projection is based on the actual area split at station 2.3. These maps show that the maximum temperature was always concentrated at the tip region of the core compressor. This is one reason that stall always began in the core compressor, as is shown in the section ENGINE RESPONSE.

Another factor that could affect the performance and distortion limits of the compressor is the shape of the instantaneous circumferential temperature pattern occurring prior to compressor stall. Figure 6 shows several patterns for each of 90°, 180°, 270°, and 360° circumferential-extent transients. The temperatures shown in this figure are the averages of the five probes on each rake at a given angular location at station 2a. The most significant characteristic of these fan inlet circumferential patterns is that the temperatures did not form a square pattern during the transients for 180°, 270°, and 360° circumferential extents. These plots show that the deviation from a square pattern is caused by the lag in the ignition of one or more burner quadrants. Specifically, quadrants 1 and 3 always lagged behind quadrants 2 and 4. The physical explanation for this lies in the lack of synchronization in opening the high-speed valves whenever more than one quadrant was fired (see the section PROCEDURE).

Pressure variations during the 90°, 180°, 270°, and 360° circumferential-extent transients are presented in figure 7 as time histories of the average fan inlet total pressure $P_{t,2}$, the average outside-wall static pressure $P_{s,2}$, and a pressure distortion

parameter defined as $(P_{t,2\text{-av}} - P_{t,2,\min})/P_{t,2,av}$. The average pressure and the minimum pressure represent data obtained from the third probe of the pressure rakes at station 2 at angular locations θ of 45°, 90°, 135°, 180°, 225°, and 270°. The plots show no appreciable circumferential pressure distortion during the transients prior to compressor stall. However, a slight increase in pressure (static and total) was observed during all attempts at producing transients with 270° and 360° circumferential extents.

In summary, the hydrogen burner delivered heated air to the fan inlet in the following conditions: (1) spatial (circumferential and radial) distortion in the temperature within the heated sectors, (2) radial and circumferential variation in the temperature rise rate, (3) a lag of quadrants 1 and 3 initial temperature rise behind that of quadrants 2 and 4, (4) very little variation in static and total pressure for $\psi < 270°$, and (5) little or no change in the instantaneous pressure distortion until stall occurred

ENGINE RESPONSE

The dynamic response of a TF30-P-3 turbofan engine to fan inlet temperature transients produced by a hydrogen burner system was characterized by one or more of the following:

(1) Instability-free operation

(2) Momentary compressor pressure disturbance

(3) High-pressure-compressor (HPC) stall

(4) Low-pressure-compressor (LPC) stall

The response was dependent on the severity of the temperature transient, as defined by the magnitude and rate of change of the fan inlet temperature, but was independent of the circumferential extent of distortion. The four sequential events are discussed separately using data obtained during transients with 180° extent at 90-percent N_1. This is followed by a discussion of the difference in compressor response between the 90- and 74-percent low-pressure-rotor speeds.

"Instability-Free" Response

An example of a 180°-circumferential-extent, "instability-free," fan inlet temperature transient is presented in figure 8 in terms of time histories of fan inlet and compressor pressures, temperatures, and mechanical speeds. The compressor was capable of tolerating transients without the occurrence of instabilities below certain levels of temperature change, depending on the circumferential extent of distortion. The magnitude of these levels is discussed in the section COMPRESSOR DISTORTION LIMITS.

It is apparent from the data shown in figure 8 that the compressor was able to readjust and return to pretransient conditions without any recognizable sign of instability. Recognizable instability is defined herein as rotating stall. During the period of the transient, the pressures and the LPC pressure ratio decreased slightly and then returned approximately to pretransient levels. The mechanical speeds (N_1 and N_2) remained constant. Fan inlet and compressor interstage temperature-time histories show that the temperatures of the unheated fan inlet sector (θ of 180° to 360°), the LPC exit at $\theta = 60^\circ$, and the HPC exit at $\theta = 120^\circ$ remained at their respective pretransient levels. The temperatures at the fan tip and hub exits at $\theta = 56^\circ$ followed approximately, with time lag, the increase in temperature of the gases in the heated sector (θ of 0° to 180°). The LPC exit (station 3) and HPC exit (station 4) temperatures remained unchanged during the 180° extent transients, although the thermocouple angular locations at these stations fall in the same circumferential location (0° to 180°) as the heated fan inlet sector. This lack of change suggests rotation of the heated gases as they pass through the compressor. This phenomenon was also observed during steady-state temperature distortion (ref. 7). To further investigate this phenomenon, time histories of fan inlet, fan tip exit, fan hub exit, LPC exit, and HPC exit temperatures during instability-free transients for 90°, 180°, 270°, and 360° circumferential extents are presented in figure 9. Again, it is apparent that only very slight changes in LPC and HPC exit temperatures occurred during 90° and 180° extent transients. However, during 270° and 360° extent transients, the temperatures at the LPC exit ($\theta = 60^\circ$) and the HPC exit ($\theta = 120^\circ$) became substantially higher than their respective pretransient levels. This would indicate that the thermocouples at these locations did not sense the hot gases from the heated fan inlet sector for the 90° and 180° extents. Based on the angular location of the thermocouples and the temperature-time histories at these locations during 90°, 180°, and 270° circumferential-extent transients, it can be concluded that the heated gases at the fan inlet rotated in the direction of rotor rotation less than 56° at the fan exit, more than 60° at the LPC exit, and more than 120° at the HPC exit. Also shown in figure 9 are the radial variations in temperature at stations 2, 2.3, 2.3f, 3, and 4. These profiles show that the maximum temperature rise ΔT shifted radially from the tip radius at station 2.3 to the mean radius at stations 3 and 4.

Momentary Compressor Pressure Disturbance

A slight increase in the magnitude and rate of inlet temperature rise above the values discussed in the preceding section resulted in a momentary compressor pressure disturbance, as indicated by $P_{s,2.6}$ and $P_{s,3}$ (fig. 10). The characteristics of temperatures and speeds were the same as those described previously. This is probably the first indication of the flow breakdown that could result in stall.

High-Pressure-Compressor Stall

A further increase in the rate $(\Delta T/\Delta t)_2$ and magnitude of inlet temperature rise $(\Delta T)_2$ above those producing momentary compressor pressure disturbances resulted in an HPC stall. A typical HPC stall, which occurred during a 180°-circumferential-extent transient, is presented in figure 11 in terms of time histories of pressures, temperatures, component pressure ratios, and rotor speeds. The first indication of the HPC stall was noted on the left side of the compressor at 76 milliseconds, as shown by the simultaneous sudden increase in $P_{t,3.12-270^\circ-1}$ and $P_{t,3-261^\circ-2}$. This was followed by the sequential stalling of the upstream stages on the left side of the compressor, as shown by the sudden increase in pressure at stations 2.6, 2.3, and 2.3f. The events occurring on the left side of the compressor were repeated on the right side of the compressor approximately 1 to 3 milliseconds later. The pressure ratio - time histories also show the initial drop of the HPC pressure ratio on the left side at approximately 76 milliseconds. This was followed by the sequential loading and unloading of the upstream stages.

The time histories of the temperatures and speeds during this HPC stall are shown in figure 11(c). These measurements were recorded on the high-speed digital system and were available only once every 10 milliseconds. Time points were connected by a straight line. The time scale is the same as in figures 11(a) and (b). The mechanical speeds and the HPC exit temperature at $\theta = 120^\circ$ remained at their respective pretransient levels during the period of the transient. The LPC exit temperature at $\theta = 60^\circ$ and the unheated fan inlet sector temperature started to increase between 70 and 80 milliseconds. This is the same time period in which the pressure traces (fig. 11(a)) show an HPC stall (76 msec). Thus, the initial increase in these temperatures is probably a result of stall. The continued increase in temperature to very high levels after stall, reaching approximately 770 K at stations 3 and 2.3, is believed to be caused by the convective motion resulting from reverse flow (ref. 8).

Low-Pressure-Compressor Stall

Very high magnitudes and rates of fan inlet temperature caused a compressor stall that began in the LPC component. A typical example of this type of response is presented in figure 12 for a 180°-extent temperature transient. The pressure-time histories (fig. 12(a)) show a simultaneous drop on the left side of the compressor of $P_{t,3.12-270^\circ-1}$ and $P_{t,3-261^\circ-2}$ at 40 milliseconds. At the same time, $P_{t,2.3-269^\circ-2}$ suddenly started to increase. This decrease and increase of pressures at stations 3 and 2.3, respectively, indicate an LPC stall that began in the stages between these two stations. This action was followed by the stalling of the fan tip component and the ap-

pearance of hammer shock at the fan inlet (station 2) on the left side. Two to three milliseconds after stall began in the left side of the LPC, stall occurred in the right side of the HPC, as indicated by the sudden increase in $P_{t,3.12\text{-}90^{\circ}\text{-}1}$ at 43 milliseconds. This was then followed by the sequential stalling of all stages upstream of station 3.12 on the right side.

The pressure ratio - time histories (fig. 12(b)) also suggest that the stall process began on the left side of the LPC, as evidenced by the sudden drop in $P_{t,3}/P_{t,2.3}$ at 40 milliseconds. The characteristics of the speed- and temperature-time histories (fig. 12(c)) were similar to those described in the preceding section for HPC stall response.

The response of the compressor during transients at 74-percent N_1 was almost the same as that which occurred during transients at 90-percent N_1. The exception was that the stall event, in most transients attempted, was preceded by an LPC rotating stall. Two examples of transients at 74-percent N_1 showing LPC rotating stall are presented in figures 13 and 14 for 90° and 360° circumferential extents, respectively.

COMPRESSOR DISTORTION LIMITS

The effects of fan inlet, time-dependent total temperature distortion on the performance and stability of the engine were probably influenced by the following variables: the low-pressure-rotor speed, the circumferential extent of distortion, the magnitude and rate of inlet temperature rise, the instantaneous spatial distortion (within the heated sector) of the absolute level of temperature, and the shape of the instantaneous circumferential wave pattern of fan inlet temperature. The last two variables were a function of the hydrogen burner system design and could not be controlled during this experiment. Also, the magnitude and rate of temperature rise were directly related as a result of the burner design. Thus, the distortion limits of the compressor can be meaningfully discussed only as a function of both the magnitude and rate of temperature rise, the low-pressure-rotor speed, and the circumferential extent of distortion. Later in this section, we will attempt to extract from the data the separate effect, for a given speed and circumferential extent, of the magnitude and rate of inlet temperature rise on the compressor distortion limits.

The compressor tolerance to time-dependent temperature distortion, as characterized by the compressor stall, is presented in figures 15 and 16 for 90- and 74-percent N_1, respectively. Plotted are the fan inlet temperature rise $(\Delta T)_2$ against the rate of rise $(\Delta T/\Delta t)_2$ for 90°, 180°, 270°, and 360° circumferential extents. Maximum fan inlet temperature rise (tailed solid symbols) and temperature rise at stall (solid symbols) are shown for transients resulting in stall. Only maximum temperature rise is shown for instability-free transients and those causing momentary pressure disturbances.

Temperature rise $(\Delta T)_2$ at stall is defined herein as the temperature rise measured in the heated fan inlet sector at the same time that peak pressure $P_{t,2.3\text{-}269^\circ\text{-}1}$ (resulting from stall propagation) occurred. The data in figures 15 and 16 show that the compressor tolerance decreased with decreasing N_1 and increased with increasing circumferential extent. For example, with 90° circumferential extent, the distortion limits decreased from 2222-K-per-second temperature rise rate and 70 K temperature rise to 1834 K per second and 59 K as the N_1 was reduced from 90 percent to 74 percent. At 90-percent N_1, the limits increased from 2222 K per second and 70 K to 3833 K per second and 117 K as the circumferential extent was increased from 90° to 360°. After a magnitude and rate of temperature rise limit were reached, compressor response (stall) was progressive, with increasingly higher magnitudes and rates of temperature rise.

The data in figures 15 and 16 also suggest the possibility of the compressor distortion limit, for a given speed and circumferential extent, being a function of a "critical" level of fan inlet temperature rise independent of the rate of rise. These possible levels are marked by a dashed line in figures 15 and 16. Further evidence of this possibility is given in figure 17, where time histories are presented of pressures on the left side of the compressor at stations 3.12, 3, and 2.3 for transients resulting in stall during 180°-circumferential-extent tests for 90- and 74-percent N_1. The symbols shown on the curves for $P_{t,2.3\text{-}269^\circ\text{-}1}$ indicate the time that the "critical" level of temperature rise (70 K at 74-percent N_1 and 78 K at 90-percent N_1) was reached. This time was calculated as $(\Delta T)_{2,cr}/(\Delta T/\Delta t)_2$. The temperature rise rate and the time of initial temperature rise ($t = 0$) were obtained as described in appendix C. Because compressor stall began in different stages of the compressor system and because stall propagation time is very short, the time when $P_{t,2.3\text{-}269^\circ\text{-}1}$ reached a peak was used to define the stall time for all data points. This time is marked by a vertical dashed line on each $P_{t,2.3\text{-}269^\circ\text{-}1}$ trace. The time from the critical level of fan inlet temperature rise to stall was then measured, and the results are plotted in figure 18 as a function of the rise rate. This difference in time is shown to be approximately constant (24 msec) and independent of the rise rate and the low-pressure-rotor speed. Thus, it can be said that these data show evidence of the independence of the compressor distortion limits from the temperature rise rate.

SUMMARY OF RESULTS

An experimental investigation was conducted to determine the effects of fan inlet, time-dependent, total temperature distortion on the performance and stability of a TF30-P-3 turbofan engine. A gaseous-hydrogen-fueled burner installed upstream of the fan inlet was used to produce the temperature transients. Data were obtained at a

fan inlet Reynolds number index of 0.50 and at low-pressure-rotor speeds of 90 and 74 percent of military speed (9525 rpm). At each engine condition, tests were conducted with 90°, 180°, 270°, and 360° circumferential extents of the fan inlet exposed to a range of magnitudes and rates of temperature rise. The following results were obtained:

1. The engine tolerance to inlet total temperature transients produced by the hydrogen burner system was a function of pretransient low-pressure-rotor speed and circumferential extent of distortion. The tolerance, as defined by the magnitude and rate of the fan inlet temperature rise $(\Delta T)_2$ required to produce compressor stall, decreased with decreasing speed and increased with increasing circumferential extent.

2. The compressor distortion limit, depending on low-pressure-rotor speed and circumferential extent, appears to be a function of a "critical" level of fan inlet temperature rise, independent of the rise rate.

3. The compressor system response to temperature transients ranged from momentary compressor pressure disturbance to low-pressure-compressor stall, depending on the severity of the distortion. Compressor stall response during transients at 74-percent low-pressure-rotor speed was, in most instances, preceded by a low-pressure-compressor rotating stall. The stall response was progressive with increasingly more severe transients at both 90- and 74-percent low-pressure-rotor speeds.

4. The heated fan inlet sector gas rotated circumferentially and shifted radially as it passed through the compressor. Circumferential rotation was more than 120° at the high-pressure-compressor exit during transients at 90-percent low-pressure-rotor speed.

5. Instantaneous spatial (circumferential and radial) distortion in the magnitude and rate of fan inlet temperature rise always accompanied the temperature transients and was primarily due to the hydrogen burner system design.

Lewis Research Center,
National Aeronautics and Space Administration,
Cleveland, Ohio, June 1, 1977,
505-05.

APPENDIX A

SYMBOLS

C	specific heat
d	thermocouple wire diameter
M	Mach number
N_1	low-pressure-rotor speed, percent of military speed
N_2	high-pressure-rotor speed, percent of military speed
P	pressure, N/cm^2
RNI	Reynolds number index, $(P/P_{sl})/(\mu/\mu_{sl})\sqrt{T/T_{sl}}$
T	temperature, K
t	time, sec
ρ	density
θ	angular location, clockwise from top dead center looking forward, deg
ψ	circumferential extent of distortion, deg

Subscripts:

av	average
cr	critical
ind	thermocouple indicated
l	left
max	maximum
min	minimum
r	right
s	static conditions
sl	standard sea-level conditions
t	total conditions
w	thermocouple wire
1	airflow-metering station
2	fan-inlet, pressuring-measuring plane
2a	fan-inlet, temperature-measuring plane

2.3	fan hub exit
2.3f	fan tip exit
2.6	middle of LPC (6th-stage stator)
3	LPC exit; HPC inlet
3.12	middle of HPC (12th-stage stator)
4	HPC exit
7	turbine exit

APPENDIX B

TEMPERATURE CORRECTION

Total temperature was measured during transients by bare-wire thermocouples with 7.6-millimeter- (0.003-in.-) diameter wire. The thermocouple-indicated temperature was corrected for time lag and ram recovery as follows:

$$T_t = \left[T_{t,\,ind} + Y\left(\frac{dT_{t,\,ind}}{dt}\right) \right] R$$

where

$$Y = -\frac{Y_0}{\sqrt{M\left(\frac{P_s}{P_{s1}}\right)}}\left(\frac{T_{t,\,ind}}{1000}\right)^{-0.18} \qquad \text{from ref. 9}$$

$$Y_0 = 1.2\,\rho_w C_w d^{3/2}$$

$$\frac{dT_{t,\,ind}}{dt} = \frac{(T_{t,\,ind})t + \Delta t - (T_{t,\,ind})t - \Delta t}{2\,\Delta t}$$

$$R = \frac{1}{1 - X}$$

$$X = 0.09072 - 0.09215\left(\frac{P_s}{P_t}\right) \qquad \text{curve fit from ref. 9}$$

where the time interval Δt is 0.01 second and P_s, P_t, and M were obtained from the steady-state data recorded prior to each transient.

APPENDIX C

CALCULATION OF FAN INLET TEMPERATURE RISE RATE

The fan inlet temperature rise rate and the time of initial temperature rise were calculated as follows:

1. The quadrant showing the maximum instantaneous temperature during the transient was identified (second quadrant during 180° circumferential extent transients and fourth quadrant during 270° and 360° extent transients).

2. The average instantaneous temperature of this quadrant was then calculated as the average of all temperature probes (10 probes) in the quadrant.

3. The instantaneous fan inlet temperature change was then calculated as the difference between the average instantaneous temperature from step 2 and the pretransient average fan inlet temperature.

4. A straight-line equation was then obtained by using the first three consecutive instantaneous temperature changes (from step 3) after the first indication of temperature rise, which produced the best straight-line curve fit using the least-squares method. The slope of the equation was defined in this report as the fan inlet temperature rise rate, and the time-axis intercept as the time of initial temperature rise.

An example of this procedure using the 180° temperature transient is shown in figure 19.

REFERENCES

1. Wallner, Lewis E.; Useller, James W.; and Saari, Martin J.: A Study of Temperature Transients at the Inlet of a Turbojet Engine. NACA RM E57C22, 1957.

2. Gabriel, D. S.; Wallner, L. E.; and Lubick, R. J.: Some Effects of Inlet Pressure and Temperature Transients on Turbojet Engines. Aeronaut. Eng. Rev., vol. 16, no. 9, Sept. 1957, pp. 54-59, 68.

3. Childs, J. Howard; et al.: Stall and Flame-Out Resulting from Firing of Armament. NACA RM E55E25, 1955.

4. Rudey, R. A.; and Antl, R. J.: The Effect of Inlet Temperature Distortion on the Performance of a Turbofan Engine Compressor System. NASA TM X-52788, 1970.

5. Armentrout, E. C.: Development of a High-Frequency-Response Pressure-Sensing Rake for Turbofan Engine Tests. NASA TM X-1959, 1970.

6. Dicus, John H.: FORTRAN Program to Generate Engine Inlet Flow Contour Maps and Distortion Parameters. NASA TM X-2967, 1974.

7. Braithwaite, W. M.: Experimental Evaluation of a TF30-P-3 Turbofan Engine in an Altitude Facility: Effect of Steady-State Temperature Distortion. NASA TM X-2921, 1973.

8. Kurkov, A. P.: Turbofan Compressor Dynamics During Afterburner Transients. Symposium on Unsteady Phenomena in Turbomachinery. AGARD CP-177, 1975, pp. 15-1 to 15-12.

9. Glawe, George E.; Simmons, Frederick S.; and Stickney, Truman M.: Radiation and Recovery Corrections and Time Constants of Several Chromel-Alumel Thermocouple Probes in High-Temperature, High-Velocity Gas Stream. NACA TN 3766, 1956.

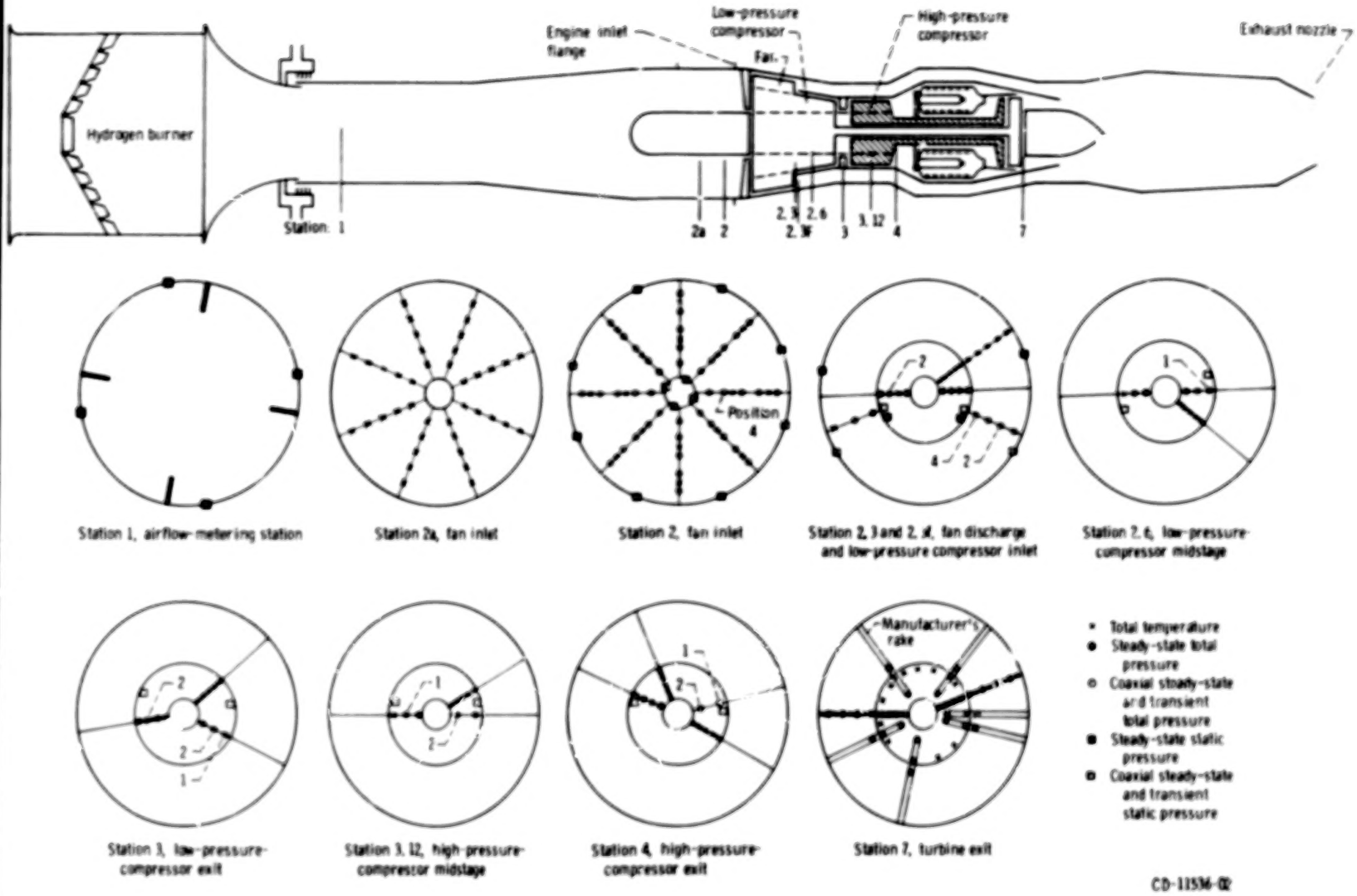

Figure 1. - Instrumentation layout for TF30-P-3 turbofan engine. (Instrumentation stations viewed looking upstream.)

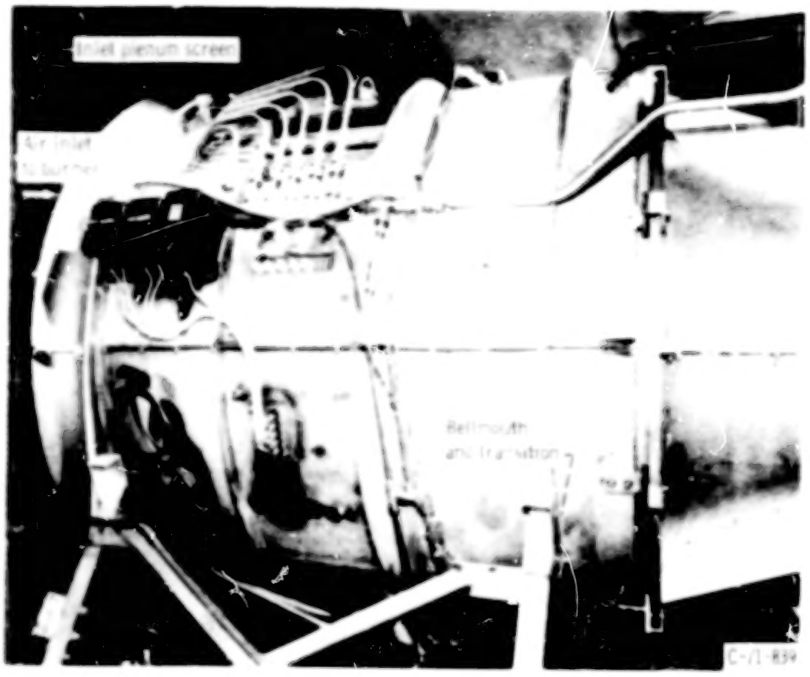

(a) External view.

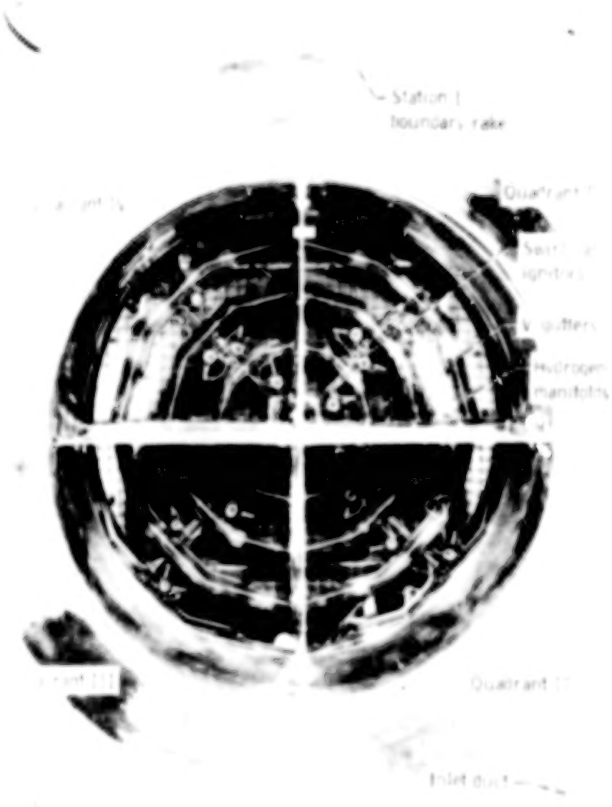

(b) Internal view looking forward.

Figure 2. - Gaseous-hydrogen-fueled burner installed in altitude chamber.

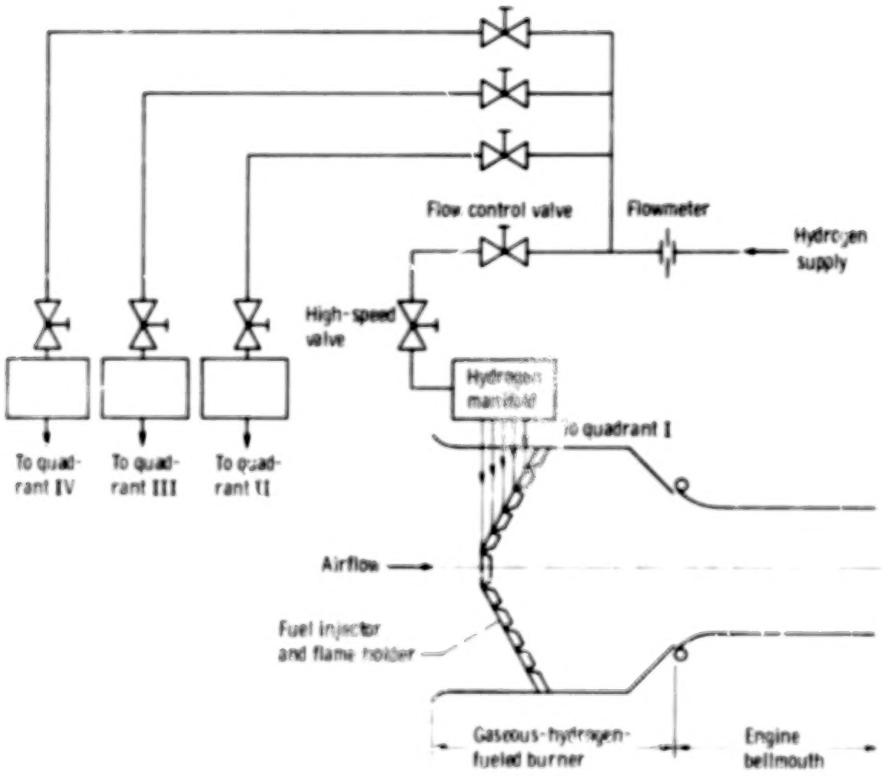

Figure 3. - Schematic of gaseous-hydrogen-fueled burner installation.

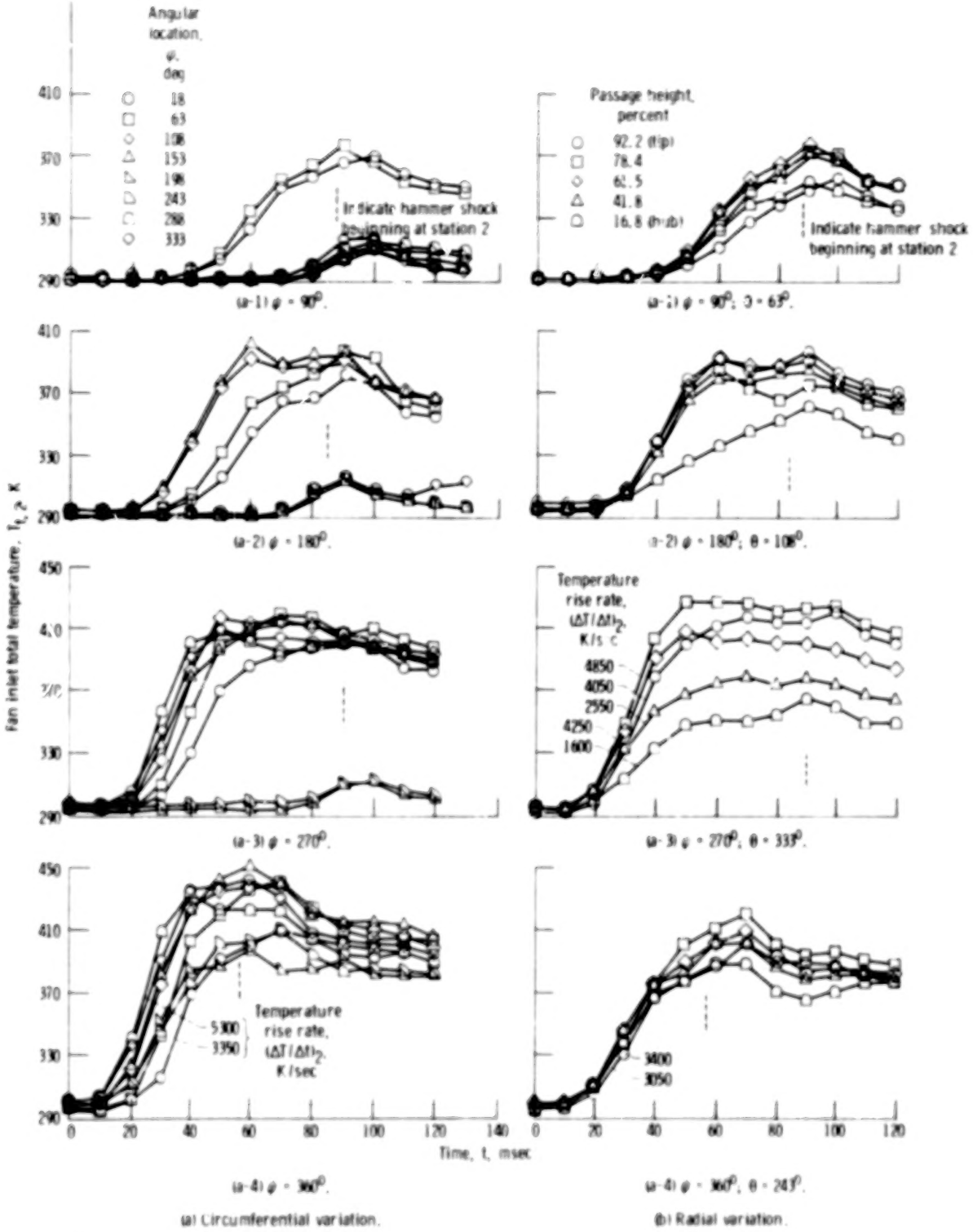

(a) Circumferential variation.

(b) Radial variation.

Figure 4. - Circumferential and radial time history of fan inlet temperature during transients at 90-percent low-pressure-rotor speed - stall conditions.

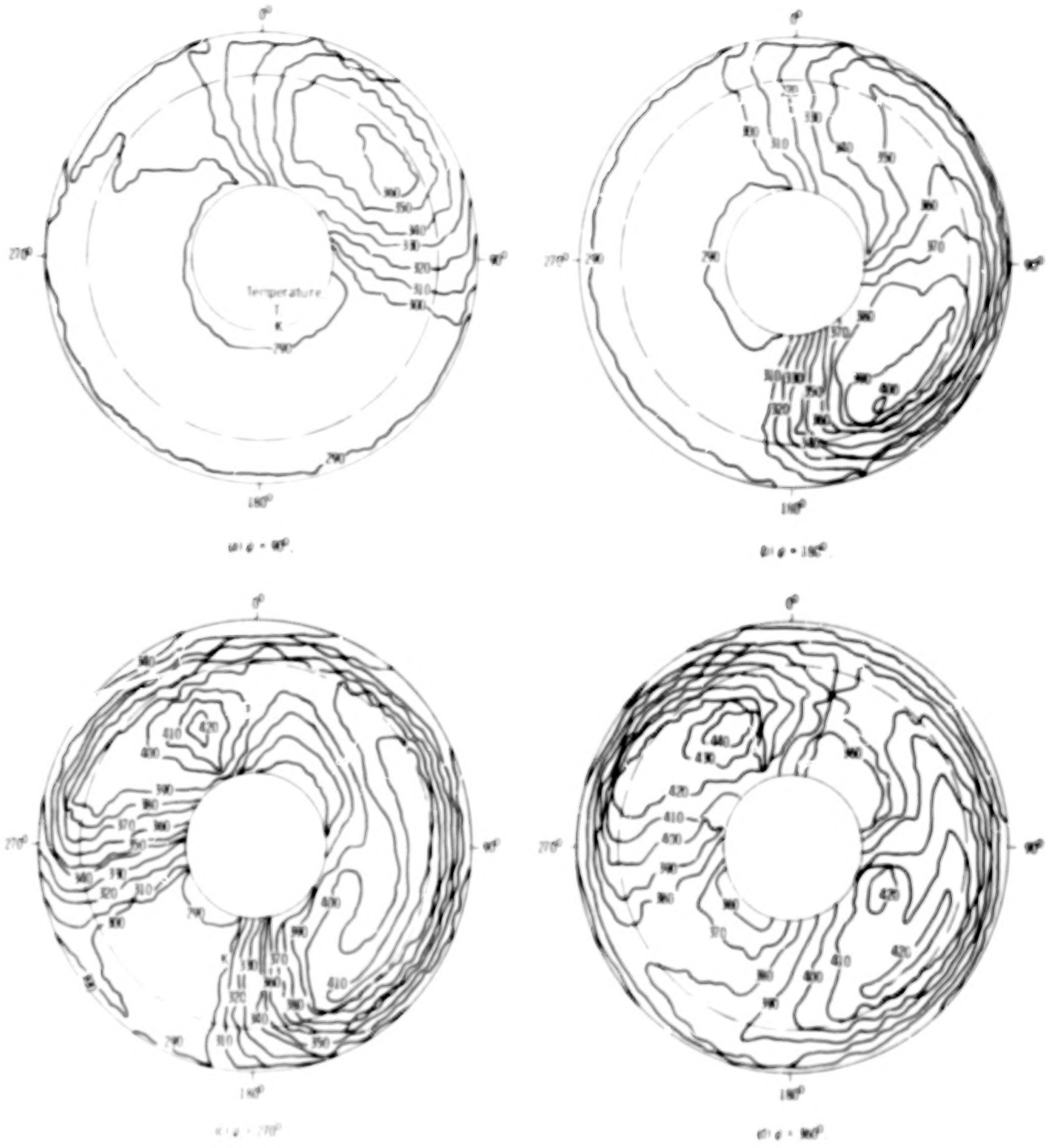
0°
90°
180°
270°
Temperature
T
K
790
810
830
850
870
890
910
930
950
970
990
1010
1030
1050
1070
1090
1110
1130
1150
1170
1190
1210
1230
1250
1270
1290
1310
1330
1350
1370
1390
1410
1430
1450
1470
1490
1510
1530
1550
1570

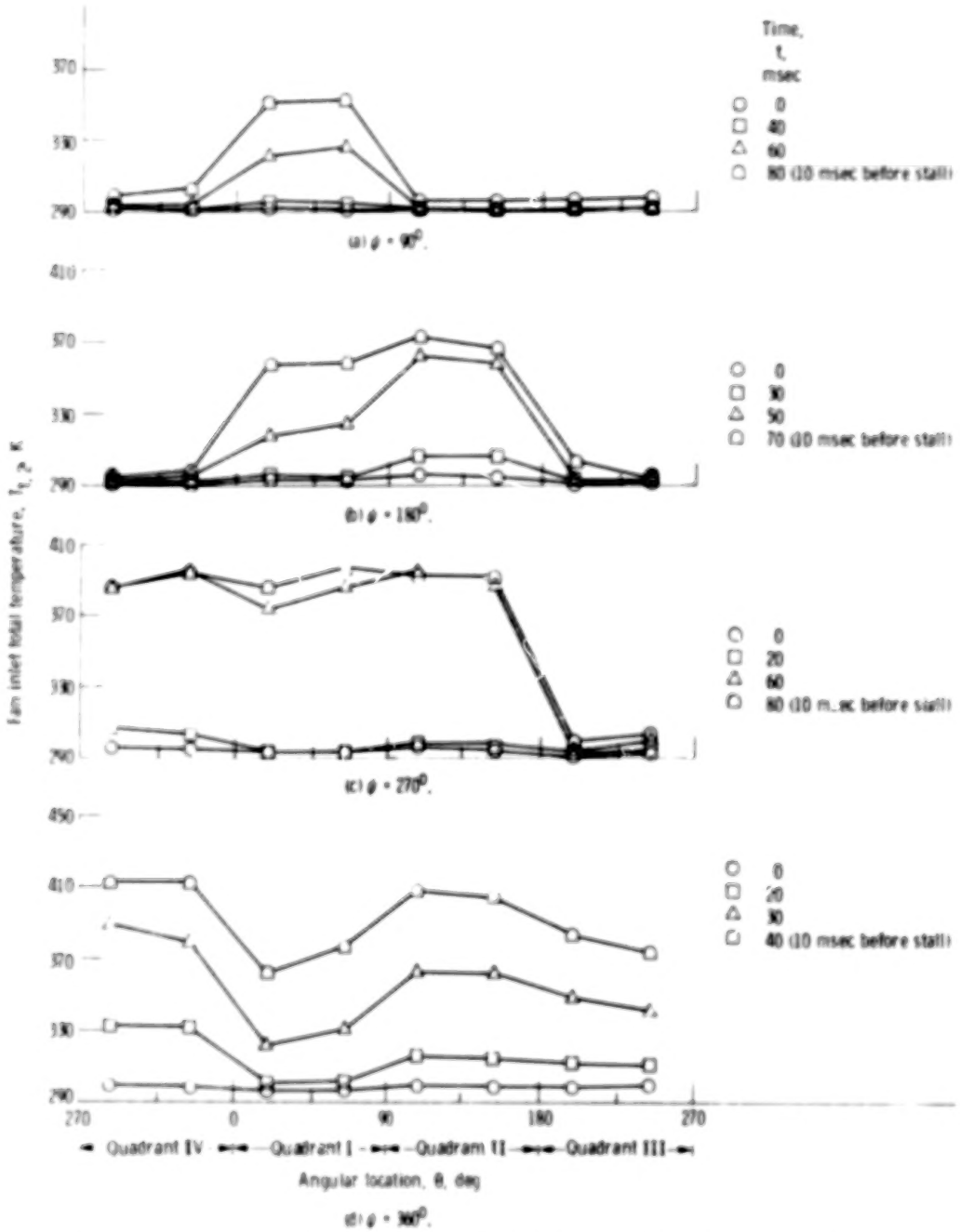

Figure 6. - Instantaneous variations in circumferential fan inlet temperature during transients at 90-percent low-pressure-rotor speed. Stall conditions.

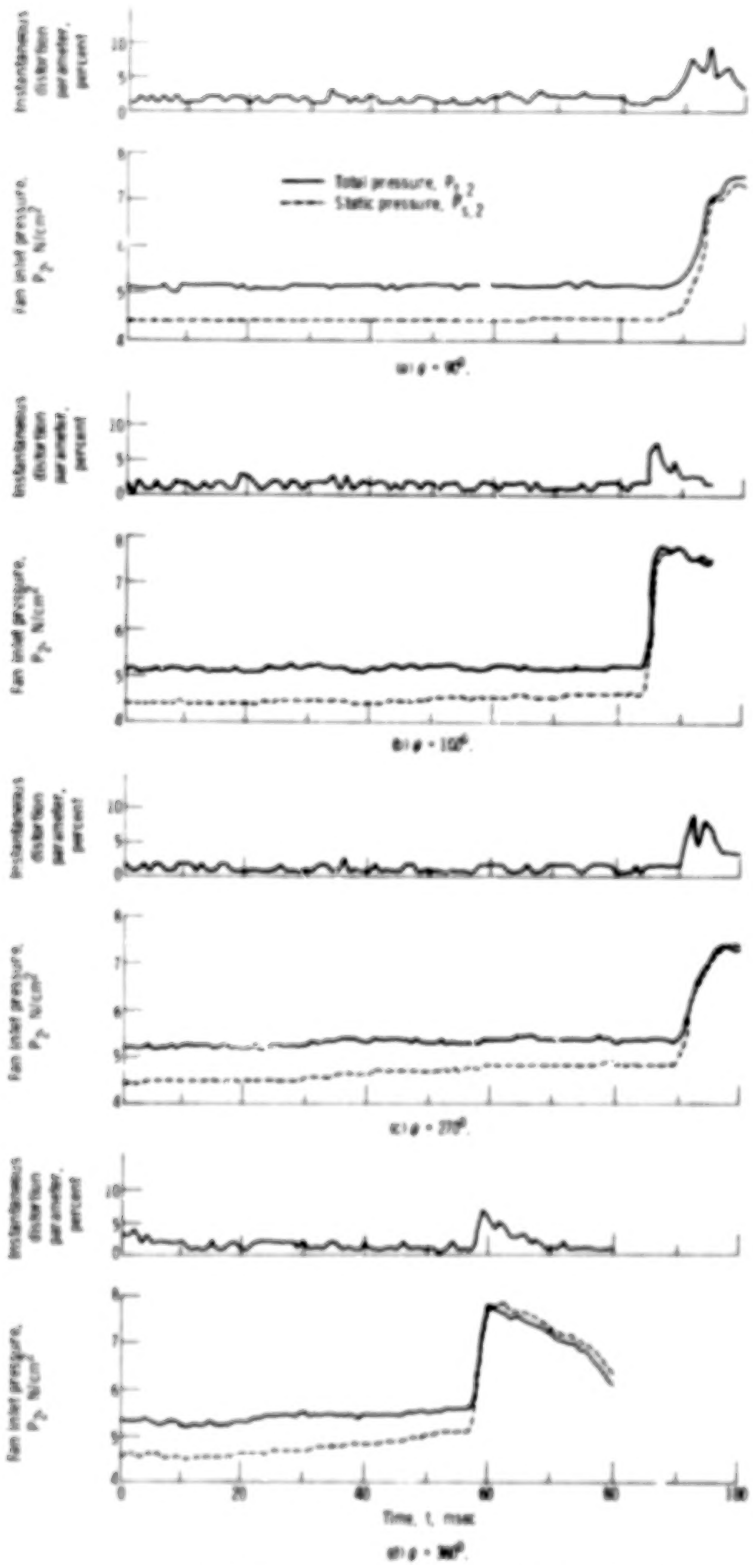

Figure 7. - Fan inlet pressure and instantaneous distortion parameter, $\theta_{t,2,av} - P_{t,2,min}/P_{t,2,av}$ variations during transients at 90-percent low-pressure-rotor speed. Stall conditions.

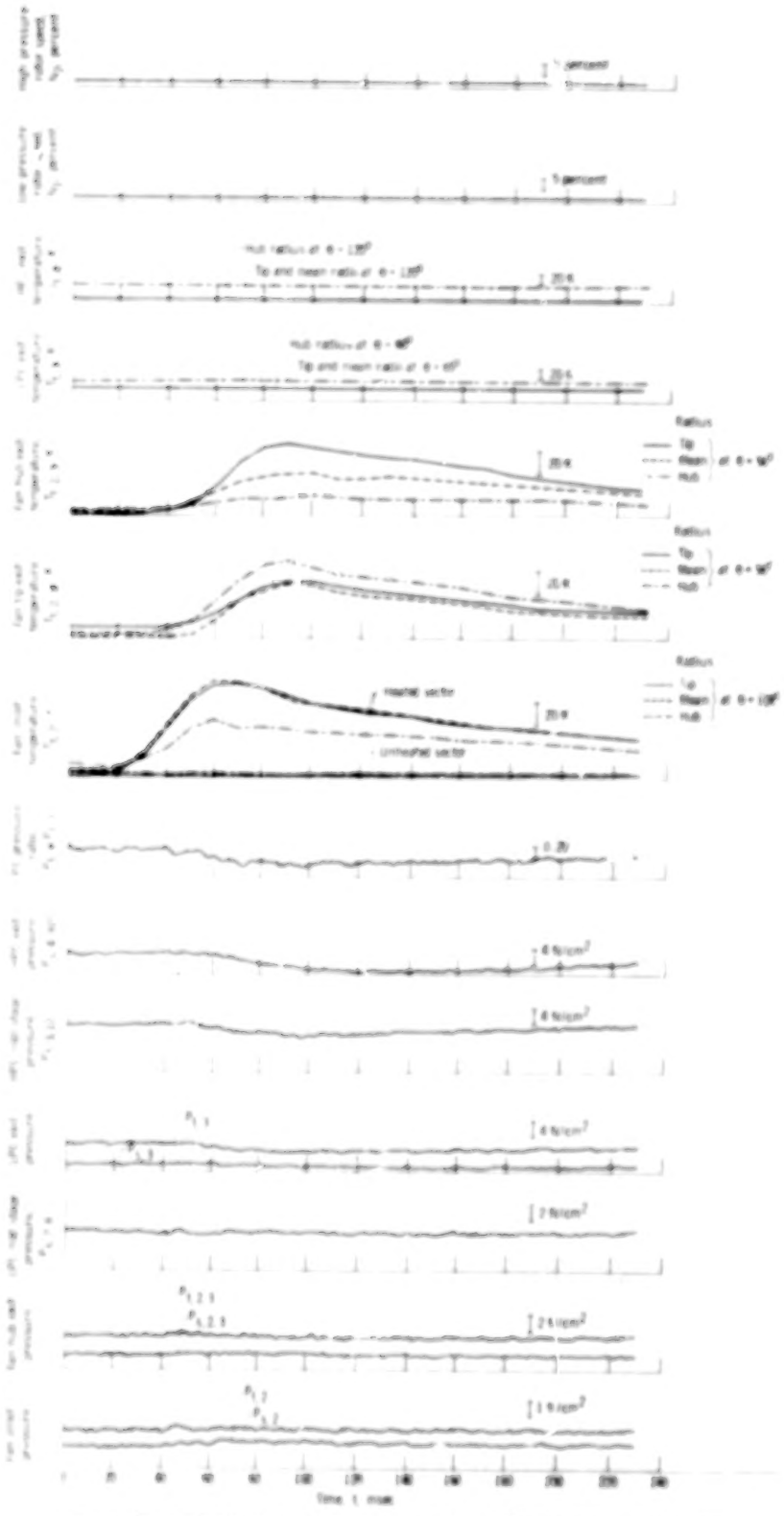

Figure 6. - Typical instability-free time history of engine parameters during 180° circumferential extent transient at 90 percent low-pressure-rotor speed. Rate of fan inlet temperature rise, dT_2/dt, 3636.4 per second; magnitude of fan inlet temperature rise, $\Delta T_{2,max}$, 59 K.

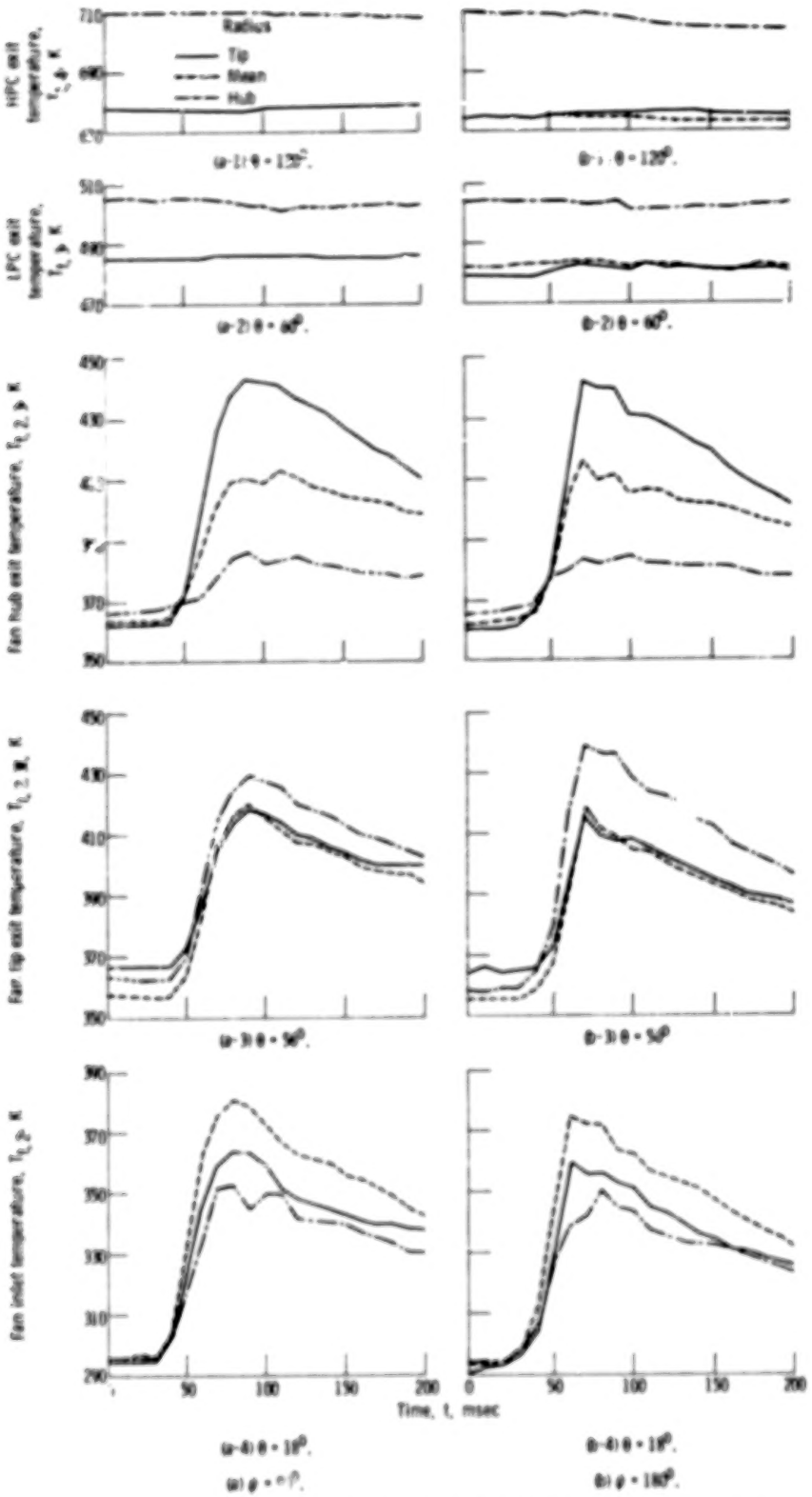

Figure 9. - Typical instability-free time history of engine temperatures at 90-percent low-pressure-rotor speed.

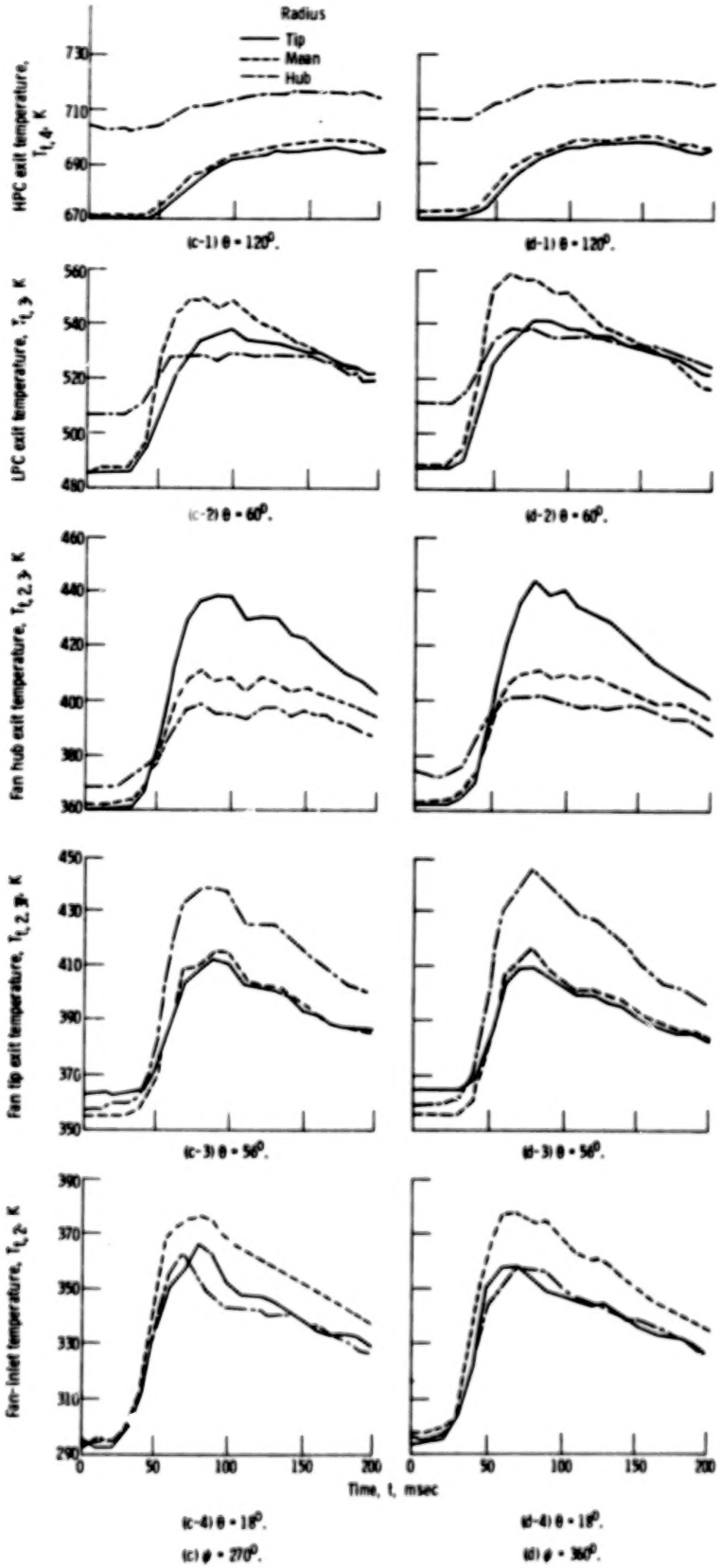

Figure 9. - Concluded.

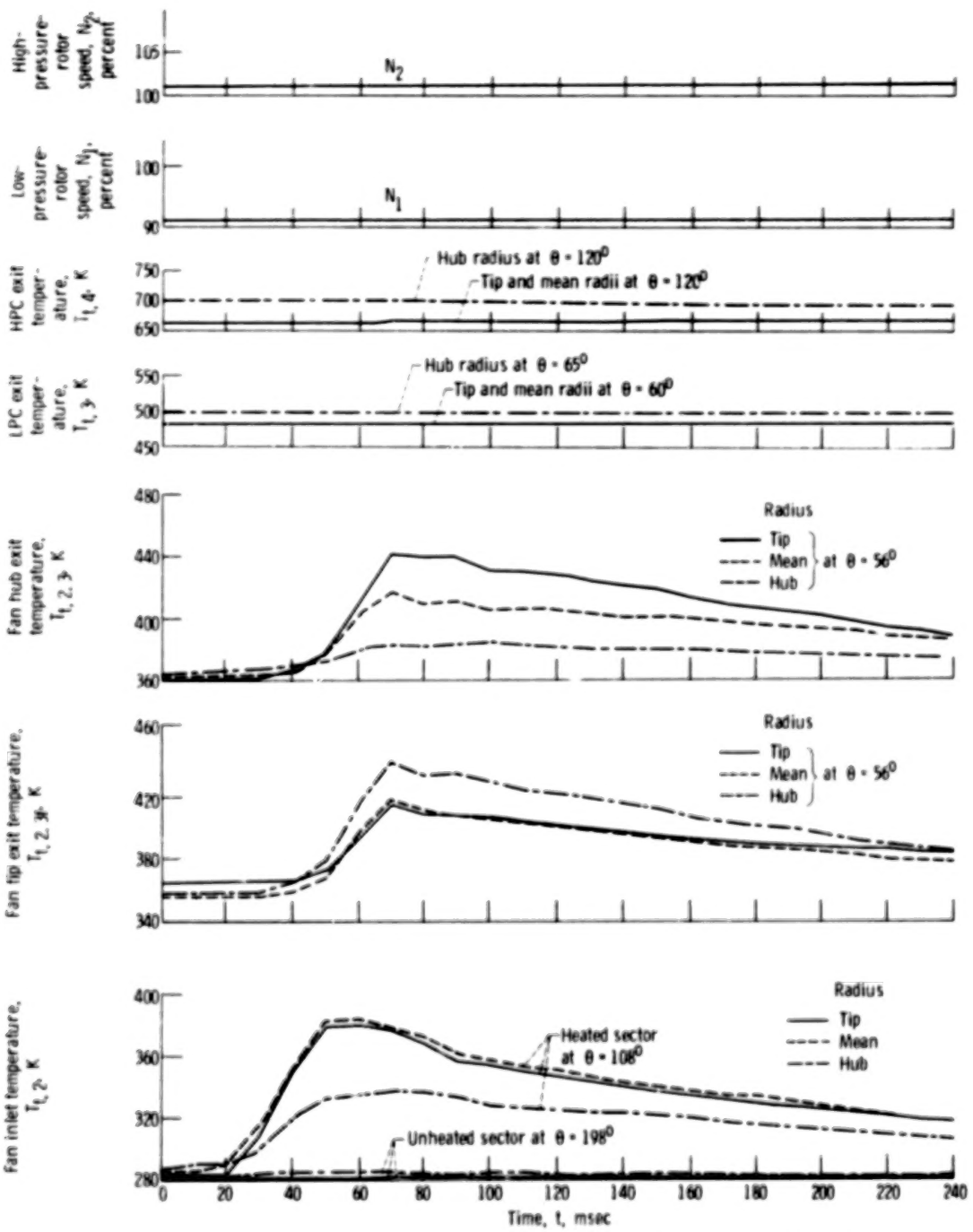

Figure 10. - Typical time history of engine parameters during 180°-circumferential-extent transient at 90-percent low-pressure-rotor speed during which a momentary compressor pressure disturbance occurred. Rate of fan inlet temperature rise, $(\Delta T/\Delta t)_2$, 2583 K per second; magnitude of fan inlet temperature rise, $(\Delta T)_{2,max}$, 74 K.

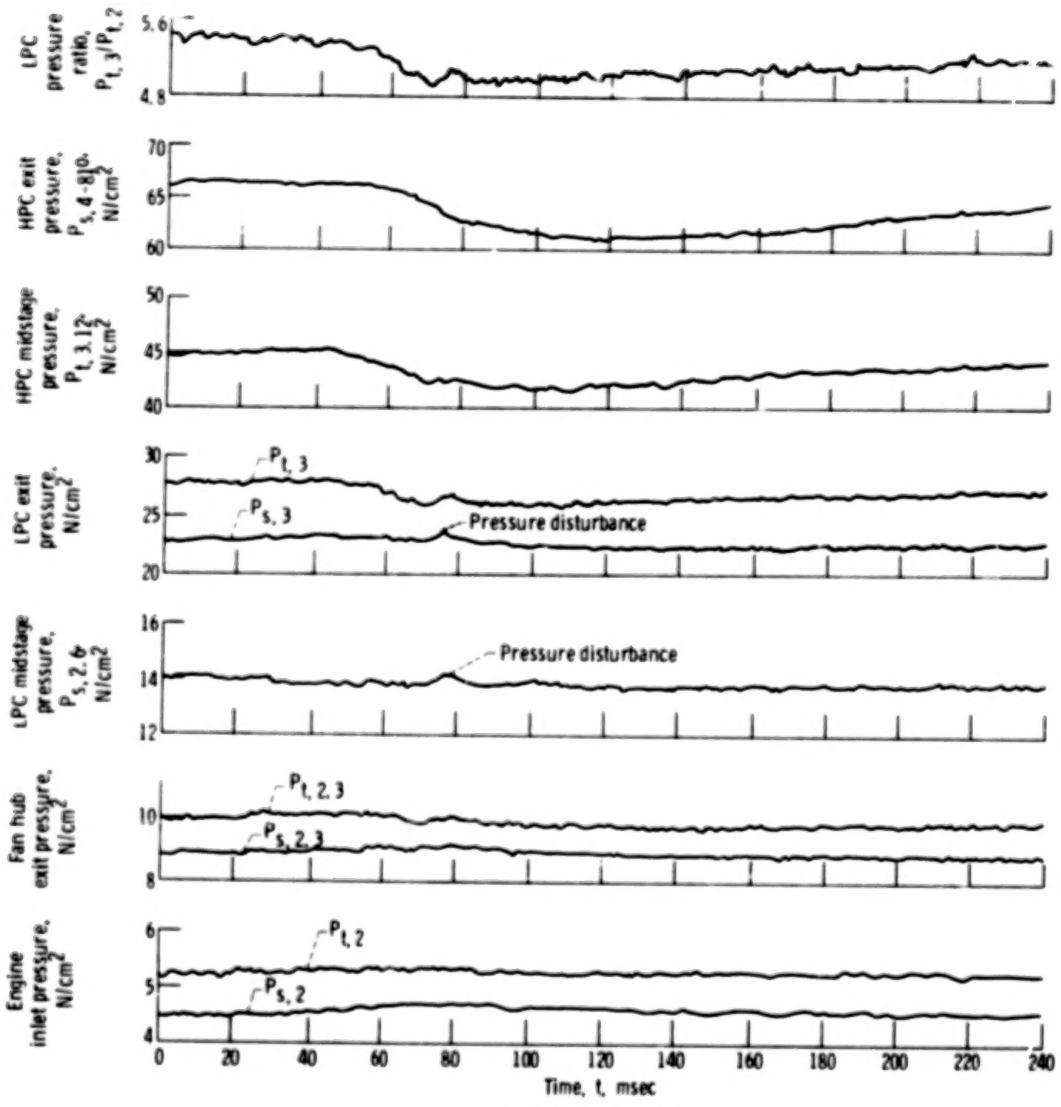

Figure 10. - Concluded.

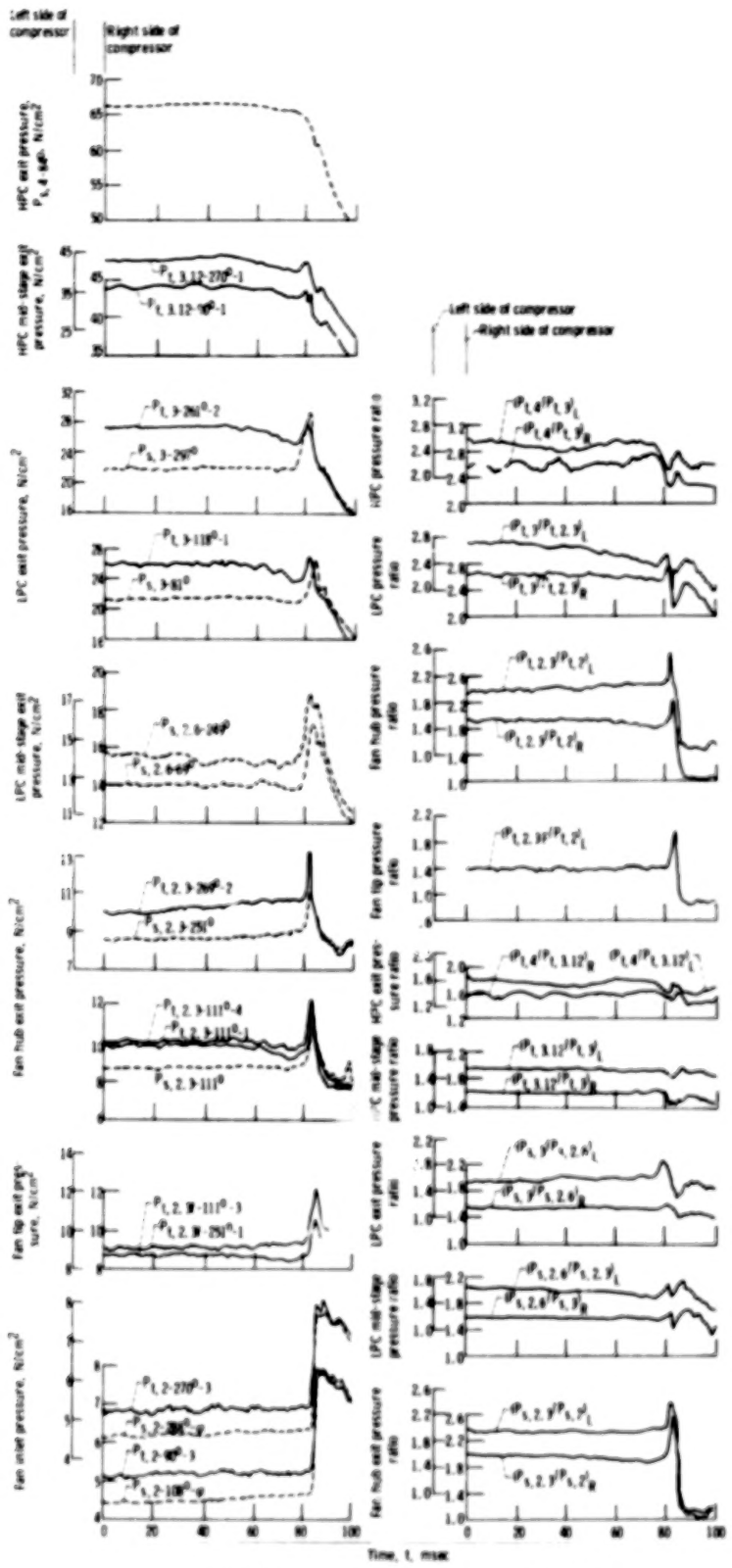
Left side of compressor
Right side of compressor
HPC exit pressure, N/cm²
HPC mid-stage exit pressure, N/cm²
LPC exit pressure, N/cm²
LPC mid-stage exit pressure, N/cm²
Fan hub exit pressure, N/cm²
Fan tip exit pressure, N/cm²
Fan inlet pressure, N/cm²
HPC pressure ratio
LPC pressure ratio
Fan hub pressure ratio
Fan tip pressure ratio
HPC exit pressure ratio
HPC mid-stage pressure ratio
LPC exit pressure ratio
LPC mid-stage pressure ratio
Fan hub exit pressure ratio
Time, t, msec
(a) Pressure.
(b) Pressure ratio.

Figure 11. - Typical time history of engine parameters during 180°-circumferential-extent distortion at 90-percent low-pressure-rotor speed during which high-pressure-compressor stall occurred. Rate of fan inlet temperature rise, $\Delta T/\Delta t_2$, 2984 K per second; magnitude of fan inlet temperature rise, $\Delta T_{2,max}$, 88 K.

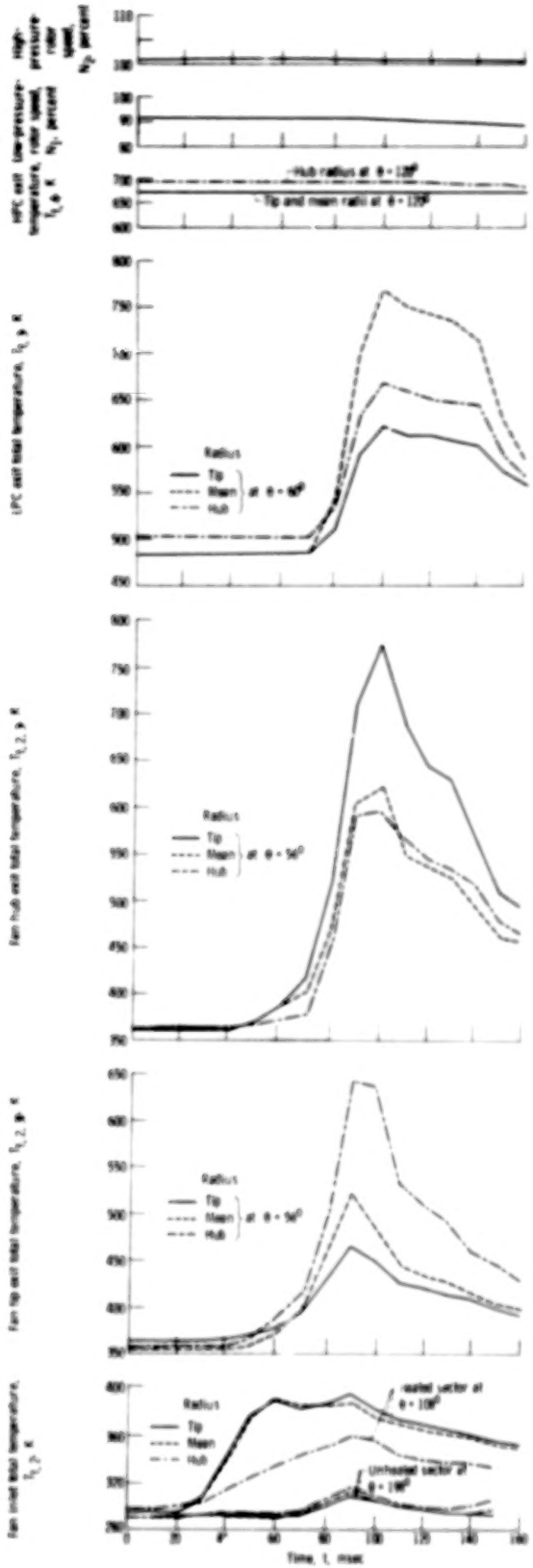
High-pressure-rotor speed, N_2, percent
Low-pressure-rotor speed, N_1, percent
HPC exit temperature, $T_{3,\theta}$, K
Hub radius at θ = 120°
Tip and mean radii at θ = 120°
LPC exit total temperature, $T_{2.5,\theta}$, K
Radius
Tip
Mean
Hub
at θ = 90°
Fan hub exit total temperature, $T_{2.2,\theta}$, K
Fan tip exit total temperature, $T_{2.2,\theta}$, K
Fan inlet total temperature, $T_{2.2}$, K
Inlet sector at θ = 108°
Unheated sector at θ = 198°
Time, t, msec

(c) Temperature and speed.

Fig. 9 11. - Concluded.

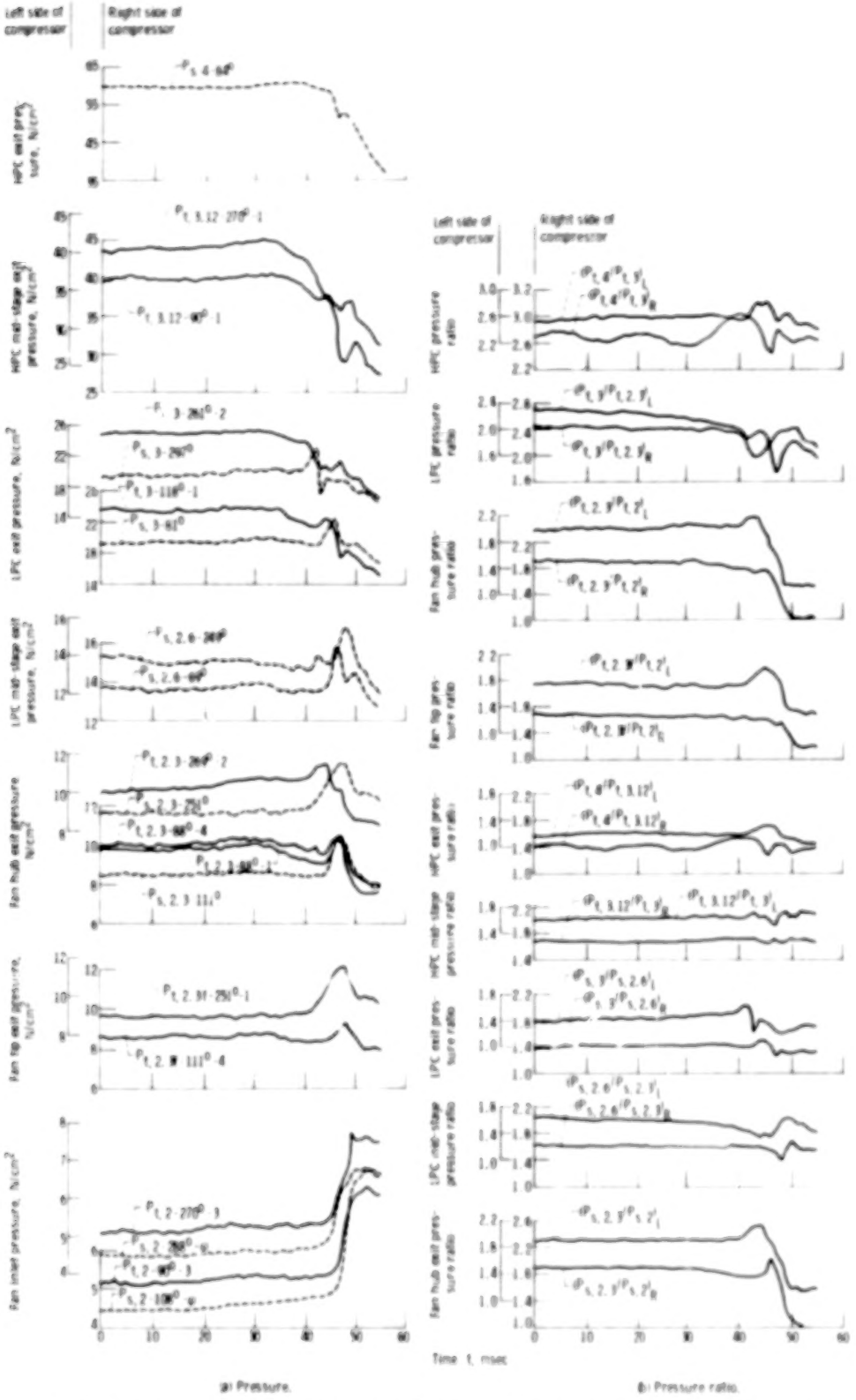
Left side of compressor
Right side of compressor
HPC exit pressure, N/cm²
HPC mid-stage exit pressure, N/cm²
LPC exit pressure, N/cm²
LPC mid-stage exit pressure, N/cm²
Fan hub exit pressure, N/cm²
Fan tip exit pressure, N/cm²
Fan inlet pressure, N/cm²
HPC pressure ratio
LPC pressure ratio
Fan hub pressure ratio
Fan tip pressure ratio
HPC exit pressure ratio
HPC mid-stage pressure ratio
LPC exit pressure ratio
LPC mid-stage pressure ratio
Fan hub exit pressure ratio
Time t, msec
(a) Pressure.
(b) Pressure ratio.

Figure 17. - Typical variation of engine parameters during 180° circumferential-extent distortion at 90 percent low-pressure rotor speed during which low-pressure-compressor stall occurred. Ratio of fan inlet temperature rise, $\Delta T/\Delta t_2$, 5990 K per second; magnitude of fan inlet temperature rise, $\Delta T_{2,\max}$, 154 K.

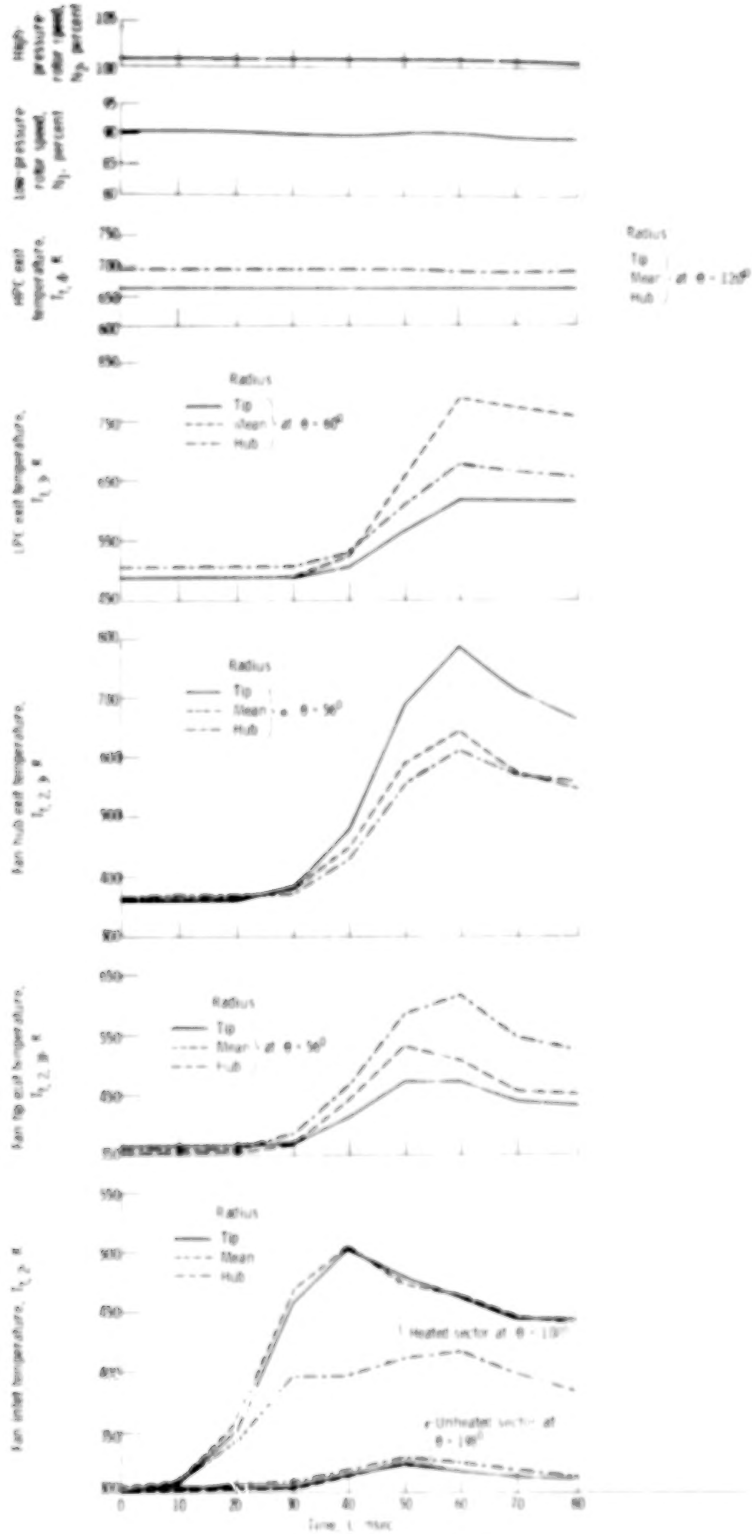

(c) Temperature and speed.

Figure 12. - Concluded.

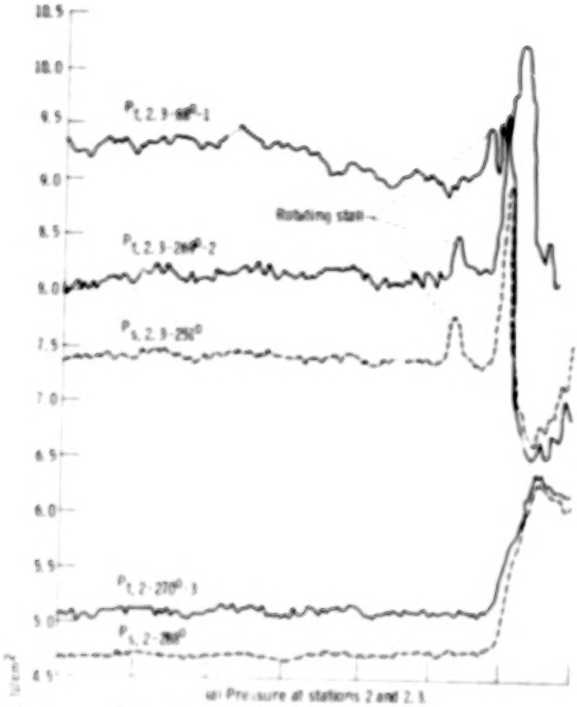

(a) Pressure at stations 2 and 2.3.

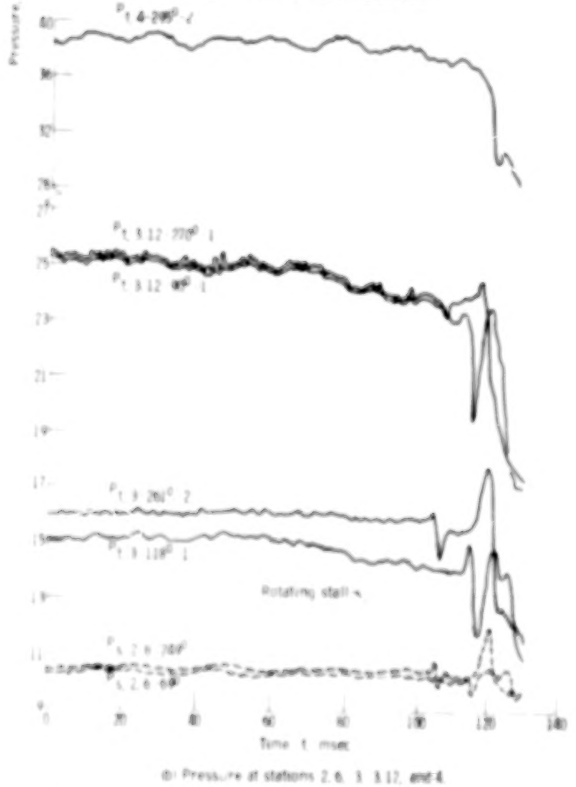

(b) Pressure at stations 2.6, 3, 3.12, and 4.

Figure 13. Typical time history of engine pressures during 90° circumferential extent distortion at 78 percent low-pressure-rotor speed during which low-pressure compressor rotating stall occurred. Rate of fan inlet temperature rise, $\Delta T/\Delta t_2$, 1816 K per second; magnitude of fan inlet temperature rise, $\Delta T_{2,max}$, 67 K.

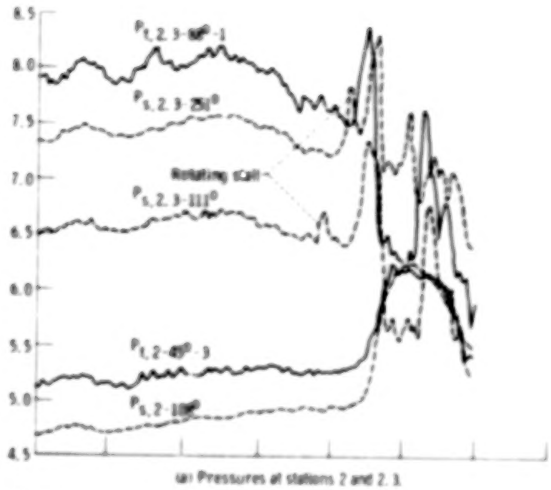

(a) Pressures at stations 2 and 2.3.

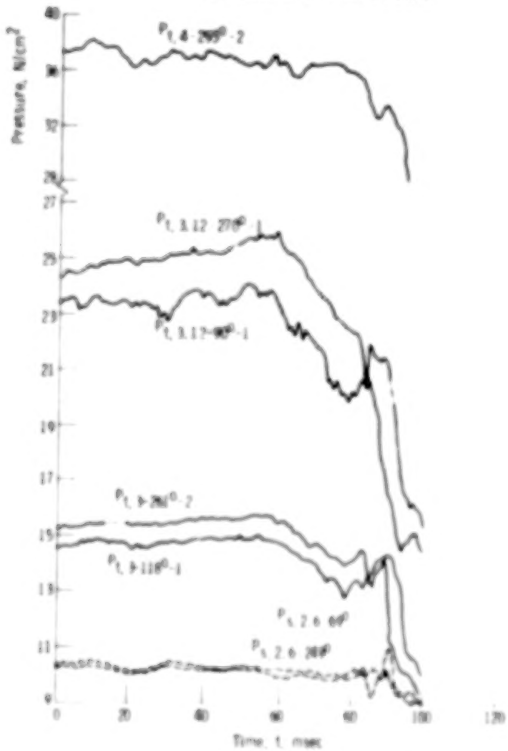

(b) Pressures at stations 2.6, 3, 3.12, and 4.

Figure 14. Typical time history of engine pressures during 90° circumferential extent distortion at 78 percent low-pressure-rotor speed during which low-pressure compressor rotating stall occurred. Rate of fan inlet temperature rise, $\Delta T/\Delta t_2$, 2666 K per second; magnitude of fan inlet temperature rise, $\Delta T_{2,max}$, 95 K.

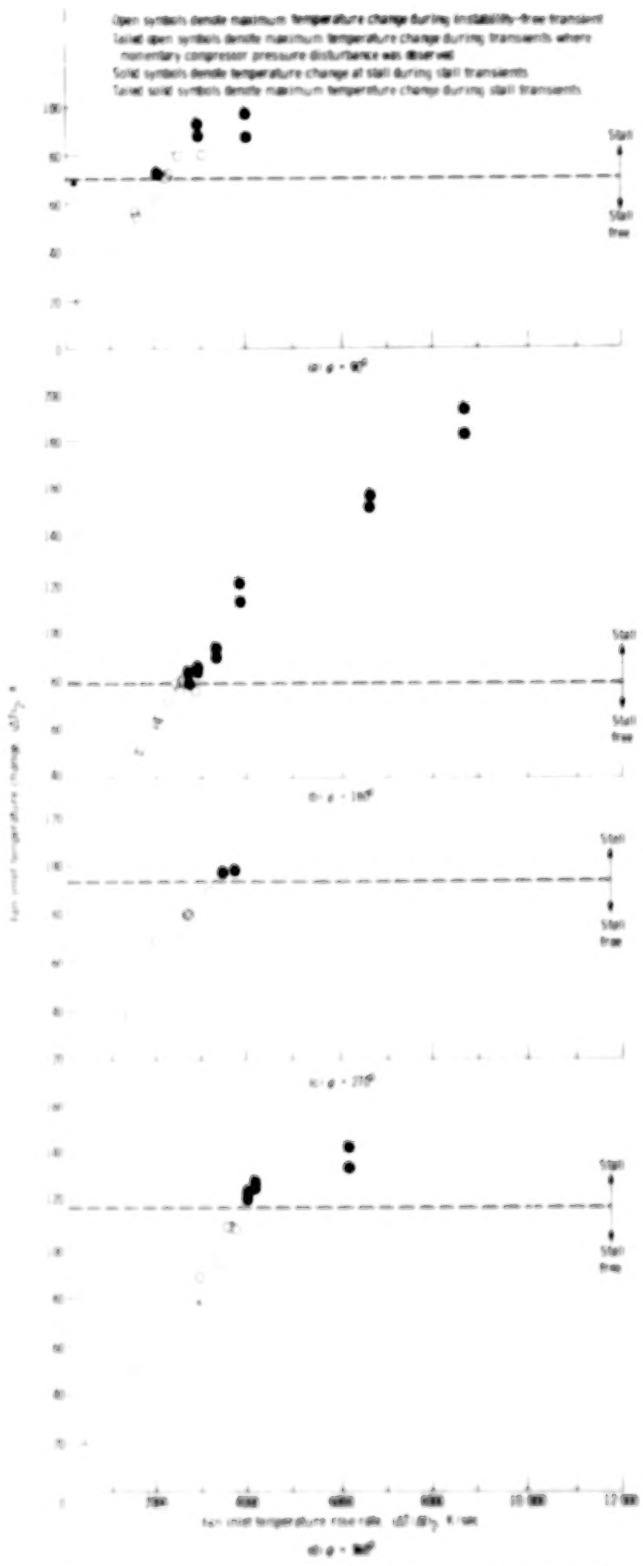
Open symbols denote maximum temperature change during instability-free transient
Solid open symbols denote maximum temperature change during transients where momentary compressor pressure disturbance was observed
Solid symbols denote temperature change at stall during stall transients
Tarred solid symbols denote maximum temperature change during stall transients
Stall
Stall free
Fan inlet temperature rise rate

Figure 15. Fan inlet temperature rise as a function of fan inlet temperature rise rate for circumferential ordent transients at 90-percent low-pressure rotor speed.

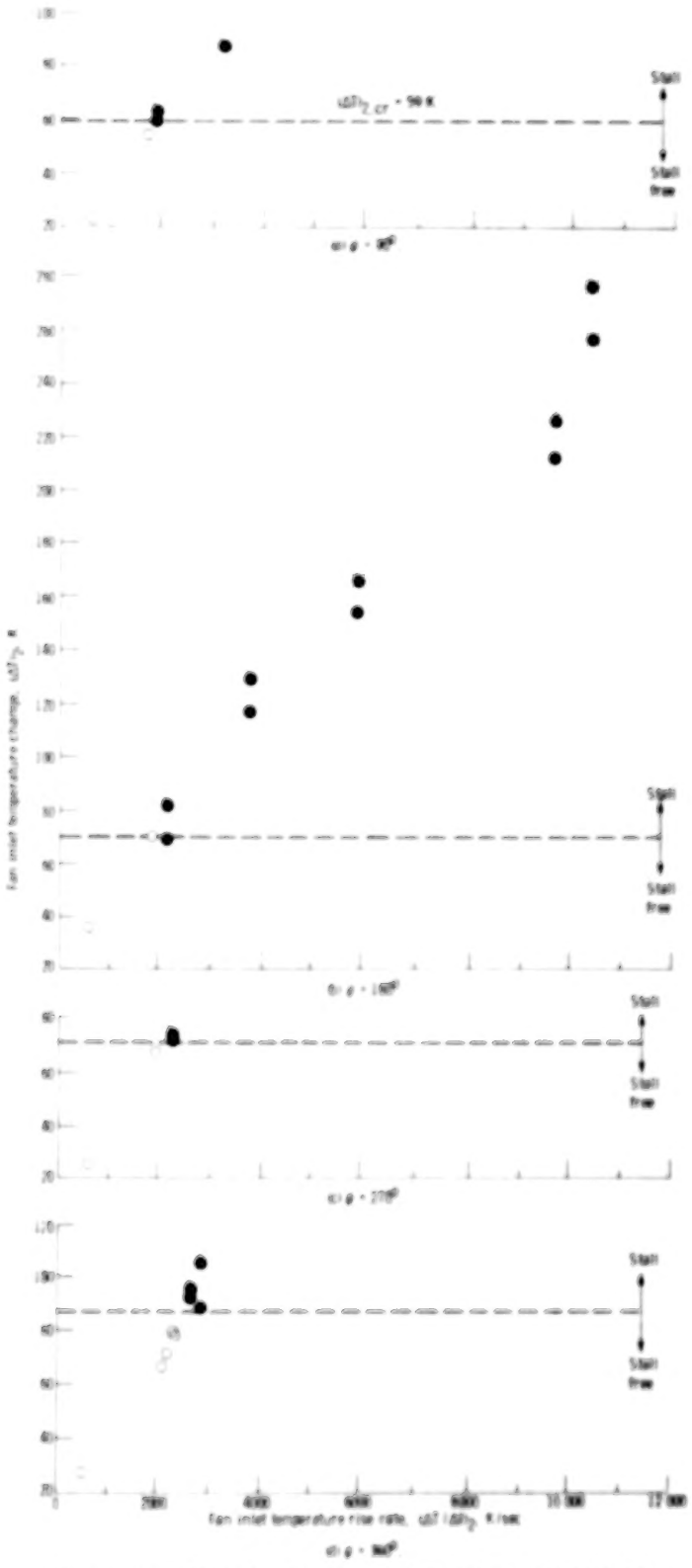

Figure 16. Fan inlet temperature rise as a function of fan inlet temperature rise rate for circumferential extent transients at 74 percent low-pressure-rotor speed.

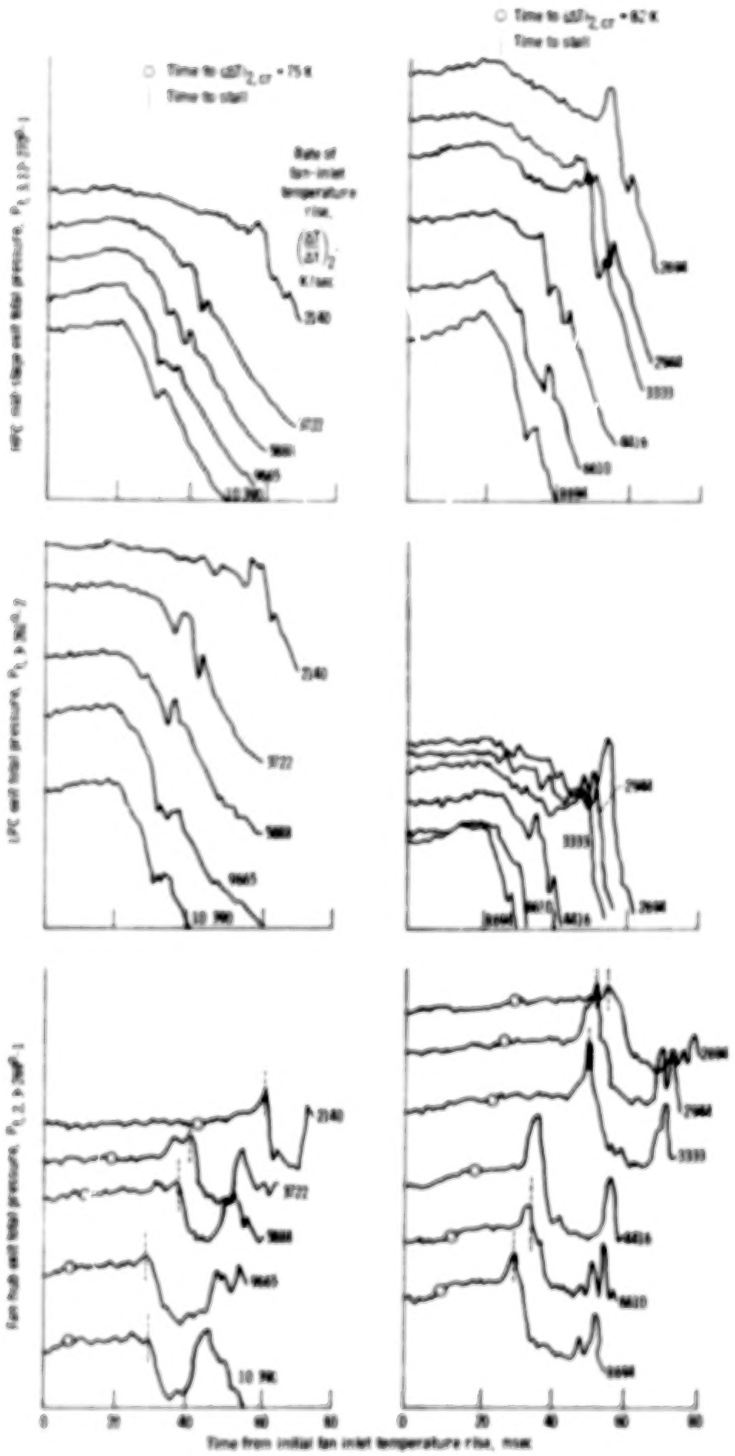

(a) Low-pressure-rotor speed, 74 percent. (b) Low-pressure-rotor speed, 90 percent.

Figure 17. - Time history of compressor pressures for 180°-circumferential-extent transients at 90- and 74-percent low-pressure-rotor speeds for different magnitudes and rates of fan inlet temperature rise - stall conditions.

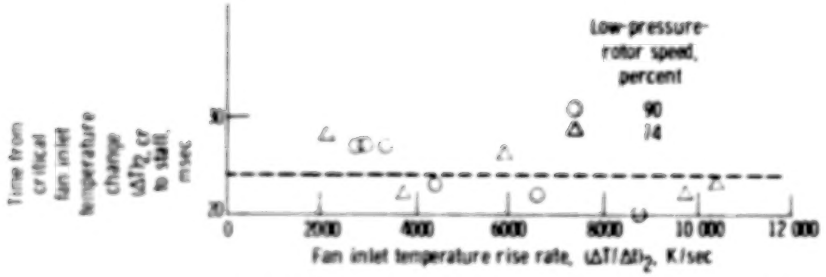

Figure 18. - Time from critical fan inlet temperature change to stall as function of rise rate for 180°-circumferential-extent transients at 90- and 74-percent low-pressure-rotor speed.

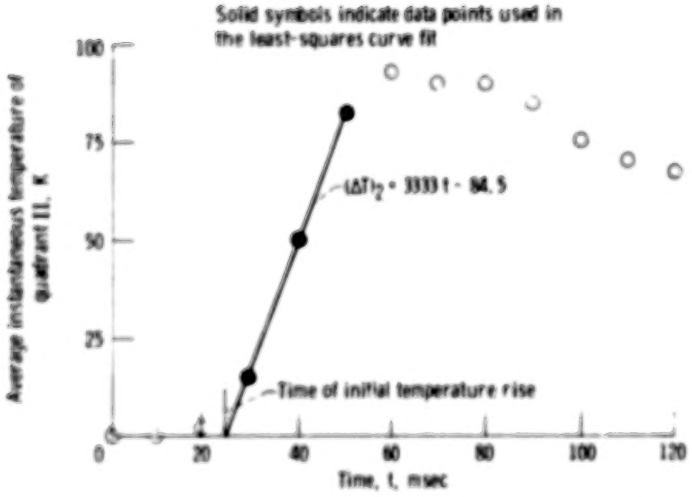

Figure 19. - Example of procedure used to calculate fan inlet temperature rise rate.

1 Report No.	2 Government Accession No.	3 Recipient's Catalog No.
NASA TP-1031		

4 Title and Subtitle	5 Report Date
EFFECTS OF TEMPERATURE TRANSIENTS AT FAN INLET OF A TURBOFAN ENGINE	September 1977
	6 Performing Organization Code

7 Author(s)	8 Performing Organization Report No.
Mahmood Abdelwahab	E-9162
	10 Work Unit No. 505-05

9 Performing Organization Name and Address	11 Contract or Grant No.
National Aeronautics and Space Administration Lewis Research Center Cleveland, Ohio 44135	
	13 Type of Report and Period Covered: Technical Paper

12 Sponsoring Agency Name and Address	14 Sponsoring Agency Code
National Aeronautics and Space Administration Washington, D. C. 20546	

15 Supplementary Notes

16 Abstract

An experimental investigation was conducted to determine the effects of fan inlet temperature transients on the performance and stability of a turbofan engine. The experiment was conducted at 90 and 74 percent of low-pressure-rotor military speed (9525 rpm) and with fan inlet temperature distortions having circumferential extents of 90°, 180°, 270°, and 360°. Temperature transients were controlled by varying the magnitude and rate of change of the inlet temperature rise. The engine response ranged from a momentary compressor pressure disturbance to low-pressure-compressor stall. The compressor distortion limits decreased with decreasing low-pressure-rotor speed and increased with increasing circumferential extent of distortion. Analysis of the data suggests strongly that the distortion limits of the compressor are a function of a critical magnitude of inlet temperature rise and are independent of the temperature rise rate.

17 Key Words (Suggested by Author(s))	18 Distribution Statement
Temperature distortion; Turbofan engine; Temperature transients	Unclassified - unlimited STAR Category 07

19 Security Classif. (of this report)	20 Security Classif. (of this page)	21 No. of Pages	22 Price*
Unclassified	Unclassified	39	A03

* For sale by the National Technical Information Service, Springfield, Virginia 22161

NASA-Langley, 1977